Fuel 381 (2025) 133383

Contents lists available at ScienceDirect

Fuel

journal homepage: www.elsevier.com/locate/fuel

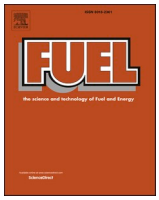

Full Length Article

Techno-economic assessment of the Allam cycle for different plant sizes, oxygen purities and heat integration with external sources

Matteo Martinelli, Paolo Chiesa, Emanuele Martelli *

Politecnico di Milano, Dipartimento di Energia, Via Lambruschini 4, Milano, Italy

ARTICLE INFO

Keywords:
Oxycombustion
Oxy-turbine
supercritical CO2 cycle
CO2 Capture
Allam cycle

ABSTRACT

This study investigates the energy and economic performance of the Allam cycle, a novel direct-fired, oxygen combustion supercritical CO_2 cycle specifically suitable for CO_2 capture and storage applications. The cycle is assessed and optimized for different plant sizes (in the range 50 MW – 400 MW of net electric power output), purity of the fed oxygen (95 %, 97 % and 99.5 % O_2 molar concentration) and heat recoverable from the Air Separation Unit and/or external processes. The analysis includes the preliminary design of the turbomachines with literature correlations for their efficiency and the detailed simulation of the CO_2 purification unit. The analysis shows that the optimal oxygen purity for the plant efficiency is 99.5 % and the net electric efficiency (including all auxiliary units) might vary in the range 48.7 % to 56.1 % depending on the plant size and heat recoverable from external processes (e.g., ASUs). The economic analysis of the cycle, performed for a 400 MW plant, indicates a promising specific total plant cost (2490 €/kW) and a competitive cost of electricity, approximately 10.4 % lower than a benchmark combined cycle with post-combustion capture system.

1. Introduction

In the last years, the development of technologies to reduce CO_2 emission into the atmosphere has been a major focus for the global research community. According to International Energy Agency [1] Carbon Capture and Storage (CCS) from power generation and industry is essential to meet the climate goals on global warming. Among the possible CCS systems, oxy-combustion represents one the most interesting routes because of two main advantages: (i) the whole flow of CO_2 rich exhausts is captured without the need of a stack and related pollutant emissions; (ii) compared to post-combustion CO_2 capture systems, chemical solvents are not required. For clean gaseous fuels, like natural gas, it is possible to use internal combustion cycles featuring a pressurized oxy-combustor followed by an expander of the flue gases. Such systems are called “oxy-turbine cycles” and there are several possible configurations. A thorough review can be found in[2]. Compared to external combustion cycles used for coal and solid fuels (e.g., see [3]), oxy-turbine cycles do not require a boiler with related savings in capital cost and the possibility of reaching higher turbine inlet temperatures with benefits in cycle efficiency. Examples of oxy-turbine cycles are the SCOC cycle [4], the Allam cycle [5,6], the Graz cycle and the CES cycle [2]. A thorough comparative analysis of the most promising oxy-turbine cycles has been performed by Amec Foster Wheeler Italiana and Politecnico di Milano [2]: the results indicate that the Allam Cycle [5,7] is the most promising in terms of net electric efficiency and cost of electricity. The cycle was patented by Allam et al. [8] in 2011 and it can be viewed as a direct-fired supercritical CO_2 cycle. In 2014, the developers presented a reheated version of the cycle [9], estimating a cycle efficiency between 59 % and 57.7 %, a power increase by 2.5 times and a limited increase in terms of capital cost [8]. In 2017 In 2018, a first-of-a-kind demonstration plant was built in La Porte, Texas [10] and the demonstration plant is currently used for equipment testing. In 2017, the cycle developers (8 River Capital) patented an improved version of the cycle featuring recompression of a fraction of the flue gases [11].

Given the novelty and very promising performance of the cycle, also academic researchers have investigated the Allam cycle. In 2016 Scaccabarozzi et al. [12] performed the first thorough optimization of the cycle efficiency. The study considered a utility scale plant (400 MWel, an oxygen purity of 99.5 % (molar basis), the basic cycle scheme without recompression of flue gases and heat recovery from the ASU main compressor cooler. Several optimized cases with different values of turbine outlet temperatures (critical value for the downstream regenerator) were considered. The most optimistic case resulted to have a net plant electric efficiency of 54.8 %.

* Corresponding author.
E-mail address: emanuele.martelli@polimi.it (E. Martelli).

https://doi.org/10.1016/j.fuel.2024.133383
Received 13 July 2024; Received in revised form 20 September 2024; Accepted 4 October 2024
Available online 14 October 2024

Nomenclature

ASU	Air Separation Unit
CPU	CO_2 Purification Unit
COE	Cost Of Electricity
COT	Combustor Outlet Temperature
HX	Heat Exchanger
IEA	International Energy Agency
LHV	Lower Heating Value
MEA	Mono Ethanol Amines
NGCC	Natural Gas Combined Cycle
O&M	Operation and Maintenance
SCOC-CC	Semi-Closed Oxy-Combustion Combined Cycle
TIT	Turbine Inlet Temperature
TOT	Turbine Outlet Temperature
T_{Ii}	Inlet temperature of the hot gas entering the i-th expander step
T_w	Maximum allowed temperature of the turbine blade wall (Nickel side)
T_{Ci}	Coolant temperature at the inlet of the i-th expander step
W_{EXP-i}	Power extracted from the i-th expander step
K_1	Calibration constant of the Aspen plus turbine model
K_2	Calibration constant of the Aspen plus turbine model
K_3	Calibration constant of the Aspen plus turbine model
m_{Ci}	Mass flow rate of the cooling flow required by the i-th expansion step
V_{Hi}	Volumetric flow rate of the hot turbine flow entering the i-th expansion step
V	Volume flow rate at the compressor inlet
Δh_{IS}	Isentropic enthalpy drop
SP	Size Parameter

The work of Scaccabarozzi et al. [12] has been used as reference (e.g., for model comparison) for a series of other simulation-based studies on the basic Allam cycle configuration (without recompression) performed by other research institutes, such as the Technical University of Graz [13], the National Research University of Moscow [14] and the University of Brescia [15]. The studies find efficiency values in the range from 50.4 % [15] to 56.5 % [14], owing to the use of different property methods (equation of states), different performance assumptions for the components, and different heat integration with the ASU.

Other research groups proposed alternative cycle configurations. For example, researchers from the University of Edinburgh [16] proposed a way of increasing the flexibility of the Allam Cycle by incorporating Liquid Oxygen Storage and a modification of the Allam cycle by recompressing an exhaust stream fraction extracted from an intermediate section of the recuperator (same idea as the one patented by 8 Rivers Capital in [11]. On one hand, the oxygen storage increases the cycle flexibility, allowing the cycle operation to be decoupled from the ASU (which represents the limiting factor, due to its very slow ramp-up rate [17]); on the other hand, the recompression of a stream drawn from the regenerator allows compensating for the heat lost without the ASU integration. The authors evaluate an efficiency of approx. 58 % for the recompressed cycle and a peak efficiency of about 66 % when the ASU is turned off (because the oxygen comes from the storage). Zhu et al. [18] proposed a modified version of the Allam Cycle called Allam-Z Cycle, where liquefied natural gas is used as fuel and liquid oxygen is assumed to be available. Indeed, LNG has a higher exergy content than natural gas at ambient temperature because it is possible to extract not only its chemical energy but also additional work from a cycle using the environment as the hot source and LNG stream as cold heat sink. Similarly, work can be produced in the regasification process of the liquid oxygen. At the described conditions, the maximum efficiency of the Allam cycle estimated by the authors is 47.90 %, while in the modified version a 50.87 % net efficiency is reached. Yu et al. [19] also studied the use of LNG as fuel for the Allam cycle, evaluating how the cold energy can be used to reduce the compression work of the cycle by means of a simulation-based optimization. Wang and Wang [20] studied the application of the Allam cycle to the natural gas pressure reduction stations, where the low-grade waste heat of the Allam cycle and ambient heat are used to heat the decompressed natural gas to the temperature required by the user. Zhang et al. [21] proposed in 2020 a recompression version of the cycle, in which a portion of the recirculated CO_2 is separated after the condenser, compressed and used in part as cooling flow and in part to balance the regenerator without the need of heat integration with the ASU. The efficiency estimated by the authors for the cycle without heat integration from the ASU is 49.34 %, which increases to 52.88 % with the use of recompression. Chan et al. [22] investigated the optimal performance of the reheated version of the Allam cycle, obtaining a net efficiency of 49.32 %, about 5 % lower than the original Allam cycle, but with a power production increase between 2.1 and 2.2 times. Wang et al. [23] proposed a new design integrating an Allam cycle with a ASU and an ammonia plant, where the nitrogen produced by the ASU serves as the feedstock for the ammonia plant to produce fertilizers. Luo et al. [24] investigated the application of the Allam cycle to a coal-fired cycle, with the adoption of a gasifier. The analysis showed an efficiency of 40.6 % with a near 100 % carbon capture. Win et al. [25] evaluated the integration of an Allam cycle with a coal-to-methanol process, obtaining a reduction of the capture energy consumption of 24.3 %, a 5.3 % fuel saving and a net power output of the system increased by 29.4 % with respect to conventional coal-based methanol production system. Xin et al. [26] studied an integrated solution consisting of a solar hybrid Allam cycle integrated with methane reforming, where CSP is used to provide heat to a solar reformer producing the syngas to be used for the Allam cycle. This configuration can achieve a net efficiency of 42.7 % and allow a fuel saving up to 10 %. To boost the efficiency above 60 %, Scaccabarozzi et al. [27] proposed a hybrid cycle, called SOS-CO_2, able to achieve a net electric efficiency of 75 % thanks to the integration of the direct-fired regenerative sCO_2 cycle with a Solid Oxide Fuel Cell (SOFC).

Other studies have focused on the design and evaluation of specific components of the Allam cycle and part-load control strategies. In 2017, Toshiba (which developed the first components for the demonstration plant) published a paper regarding the design and development of the turbine and compressor of the demonstration plant [28]. In 2019, Scaccabarozzi et al. [29] proposed a 1-D model for the preliminary design of the Allam cycle turbine, able to assess the number of stage, loadings, velocity triangles, fluid-dynamic performances and cooling flow requirements and impact on the overall performance. A preliminary study of the turbine design is reported also in [14]. Scaccabarozzi et al. [30] evaluated the part-load performance of the Allam cycle and proposed an efficient part-load control strategy. The part-load analysis was then continued by Zaryab et al. [31] proposing and comparing different effective control strategies. The results indicate that, thanks to the regenerator and the possibility of adapting the turbine outlet pressure, the Allam cycle features a limited decay of efficiency at part-loads, making it suitable for flexible operational schedules.

Despite the large number of technical studies on the Allam cycle, several research gaps still need to be addressed. One of the first gaps concerns the selection of the most accurate equation of states to model the Allam cycle. The second research gap is the influence of the oxygen purity on the efficiency and optimal cycle parameters for the Allam cycle. A third very important research question is the effect of the heat

integration (i.e., heat received from the ASU or external heat sources) on the optimal cycle parameters and efficiency. As forth point, no previous study assesses the effect of the plant size on turbomachines and cycle efficiency. Finally, none of the previous literature studies performs an economic analysis based on the detailed sizing of the cycle components (compressors, turbine, recuperator, CO_2 purification unit, intercoolers, condenser, etc.). This work consider the basic scheme of the Allam cycle (i.e., the version without recompression) and addresses these four research questions. In particular, this work uses detailed models of the Allam cycle and its components with the goals of:

- Assessing the effects of oxygen purity on the cycle performance
- Evaluating the effect of the heat integration between ASU and recuperator on the cycle performance
- Assessing the effect of the plant size on the cycle performance.
- Estimating the economic key performance indicators of the Allam cycle and comparing it with a benchmark post-combustion CO_2 capture technology.

A future work will repeat the same analysis for the Allam cycle scheme with recompression (the scheme patented in ref. [11].

2. Allam cycle scheme and considered cases

2.1. Allam cycle scheme

In this work we focus on the original Allam cycle scheme, as published by the inventors in the first papers [57], also adopted in the IEA Report [2] and in [12]. The scheme is reported in Fig. 1. It is important to notice that different plant arrangement have been proposed in literature (see, e.g., the modified configuration with recompression proposed in [9]) and the results found in this work cannot be extended directly.

Nearly pure oxygen (99.5 %mol purity) (stream 17) pressurized at 120 bar is supplied by a cryogenic air separation unit (ASU) and then it is mixed with a stream of recycled CO_2 (stream 16), preheated to approximately 705 °C in the regenerator (REG) and sent to the combustor (stream 4). Oxygen is mixed with CO_2 for safety reasons since pure oxygen becomes extremely corrosive and chemically active against materials above 200 °C [32] before being preheated in the regenerator and for reducing the temperature of the diffusion flame. To limit safety and corrosion issues, the concentration of O_2 is lowered below 30 %. In the case of the Allam cycle, the cycle developers consider a concentration of 25 % [7] while Amec Foster Wheeler considers a safer concentration of 13.3 % [2].

The combustor operates at supercritical pressures (i.e., above the critical pressure of the CO_2 rich stream), preferably between 200 bar and 400 bar and the firing temperature is moderated by injecting a large recycle stream of CO_2 (stream 5). Hot combustion gases (stream 6) at temperatures above 1050 °C enter a cooled turbine (TUR) featuring a limited expansion pressure ratio, between 6 and 12. Flue gases at temperatures of approximately 720–730 °C and a pressure ranging from 30 to 60 bar depending on the case enter a multi-flow heat exchanger (here called “regenerator”, REG) which allows recovering the available heat by preheating the recycle streams (streams 4, 5) as well as the turbine cooling flows (stream 7). At the exit of the regenerator, the exhaust stream (stream 9) is cooled close to ambient temperature in a cooler (CON) which condenses and separates the water (stream 23). The remaining stream (#10) is highly concentrated CO_2 in the gas phase. Part of this stream is separated and sent to CO_2 purification, compression and storage (stream 22), while the majority (stream 11, approximately 95 % of 10) is compressed and recycled back to the combustor as temperature moderator. The intercooled compressor pressurizes the recycle stream to about 80 bar (above the critical pressure) and the aftercooler takes it to near ambient temperature. Since these conditions (stream 12) are supercritical (dense phase CO_2) and correspond to a very high density of about 700 kg/m^3, the compression from 80 bar to the combustor pressure is performed with centrifugal dense-phase compressors (CPR-5, CPR-6, and CPR-O). The ASU is thermally integrated with the cycle: the heat available by cooling the air stream after the main

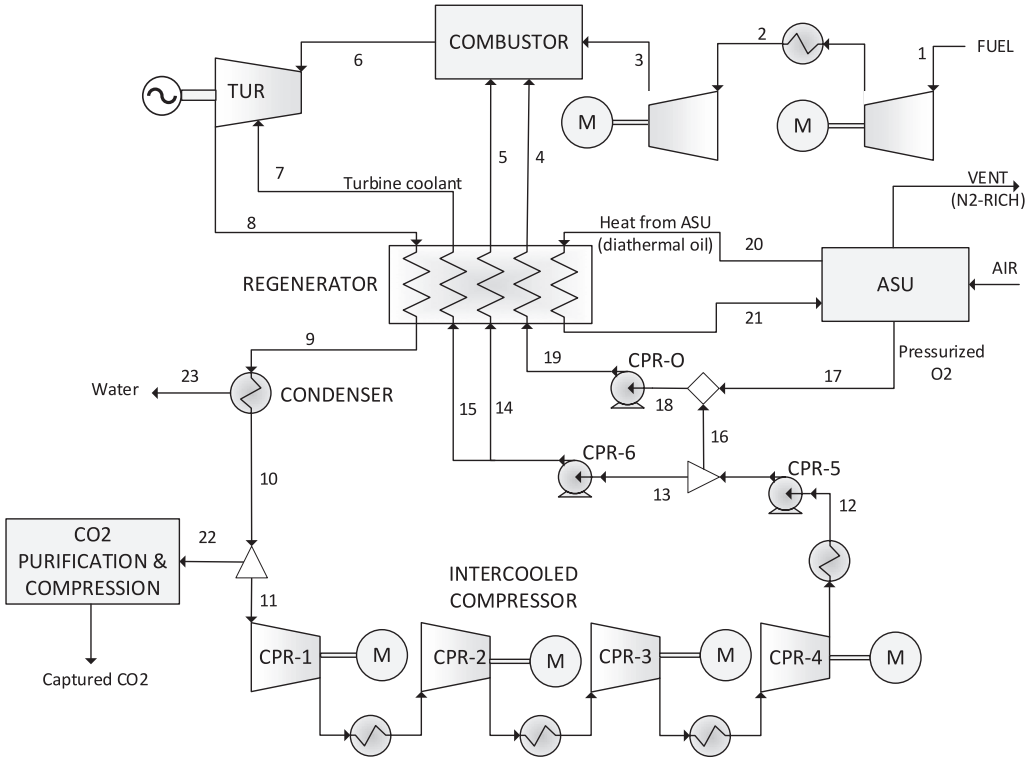

Fig. 1. Process flow diagram of the Allam cycle scheme considered in this work.

compressor is supplied to the regenerator by means of a diathermal oil loop which is assumed to reduce the available heat temperature by 20 °C.

2.2. Design cases and sensitivity analyses

For the base cycle configuration shown in Fig. 1, the effects of plant size, oxygen purity and heat integration with the ASU on the plant performance are investigated by means of sensitivity analyses. The cases investigated in this work are summarized in Table 1 and Fig. 2. Case BC is the base case design resembling the one already optimized by Scaccabarozzi et al. [12] for 50 Hz utility scale plants. Its size of 400 MW net electric plant output corresponds to the maximum size of a single train of air separation unit. The ASU provides high purity oxygen (99.5 % molar basis in the base case, although other purities have been investigated in the sensitivity analysis detailed in Section 6) and medium temperature heat recovered from the aftercooler of the main air compressor. It is representative of a utility-size Allam cycle.

Cases PS-300, PS-200 and PS-100 are aimed at assessing the effect of plant size on the efficiency of the Allam cycle. The only difference between these cases and case BC is the size of the components. Case PS-50 denotes a very small size plant employing an uncooled turbine. It allows assessing the effect of adopting a lower turbine inlet temperature and more conservative turbine design on the efficiency of the Allam cycle. Cases OP-95 and OP-97 are considered to assess the influence of the oxygen purity provided by the ASU on the cycle design and efficiency. These cases have the same design criteria and size as the base case except for the purity of oxygen provided by the ASU. Finally, cases AHI-NO and AHI-AD are variations of the utility scale case (BC) assessing the effect of the heat integration with the ASU: in case AHI-NO, there is not heat integration between the ASU and the Allam cycle, while in case AHI-AD the heat integration scheme is enhanced by recovering heat from the booster air compressor and other sources.

3. Cycle modelling and methodology

3.1. Equation of state

The first step required for the Aspen Plus modelling is the selection of an appropriate equation of states (EoS). Considering the working fluid composition and operating conditions of the Allam cycle, real gas effects are expected to occur in the high pressure low temperature streams at the inlet of the compressors and regenerator. In order to properly assess the cycle efficiency (i.e., required heat input and power for compression/expansion), the EoS has to predict the specific volume (as a function of pressure and temperature) and specific heat of the CO_2-rich

Table 1
Summary of the analyzed cases.

	ASU O2 purity (mol. basis)	ASU heat integration	Net plant size	Turbine cooling
BC	99.5 %	heat recovery from main air compressor aftercooler	400 MWel	yes
PS-300	99.5 %	heat recovery from main air compressor aftercooler	300 MW	Yes
PS-200	99.5 %	heat recovery from main air compressor aftercooler	200 MW	Yes
PS-100	99.5 %	heat recovery from main air compressor aftercooler	100 MW	yes
PS-50	99.5 %	heat recovery from main air compressor aftercooler	50 MW	no
OP-95	95 %	heat recovery from main air compressor aftercooler	400 MW	yes
OP-97	97 %	heat recovery from main air compressor aftercooler	400 MW	yes
AHI-NO	99.5 %	No heat integration with ASU	400 MW	yes
AHI-AD	99.5 %	Heat recovery from main air compressor and other sources	400 MW	yes

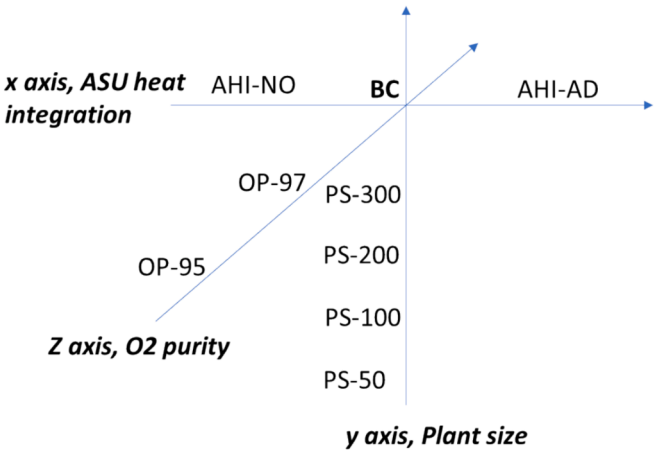

Fig. 2. Summary of the cases considered in the three sensitivity analysis of this work: sensitivity analysis on the plant size (vertical y axis), heat integration degree with the ASU (horizontal x axis) and O2 purity (z axis).

mixtures with high accuracy. While experimental data for the specific volume of CO2-rich mixtures similar to those of the Allam cycle are available in literature (see Table 2), no experimental data are available on the specific heat capacity of CO2-rich mixtures relevant for the Allam cycle. Thus, the accuracy of the equation of states has been selected looking only at the accuracy in predicting the specific volume. Table 2 reports a summary of the conditions of each experimental source in terms of measured property, composition, interval of temperature and pressure of the measurement, number of evaluated experimental points and reference. The selected candidate equations are the Peng-Robinson, the Soave-Redlich-Kwong, the Benedict–Webb–Rubin–Lee–Starling, the Lee-Kesler-Plöcker and the GERG-2008.

The evaluation of the performance of the equations of states is carried out by simulating with Aspen Plus the experimental points with each of the equations of states, evaluating the average error made with respect to the experimental data. The results of the procedure are reported in Table 3: it can be seen how the GERG-2008 equation of states has not only the lowest overall average error, but also the lowest average error for each of the studied mixtures apart from the cases A1 and NA2. For this reason, the GERG-2008 has been selected to model the Allam cycle (power block).

As far as the CPU is concerned, the equation of states must predict not only the specific volume and specific heat capacity, but also the composition of the two-phases in the vapor–liquid equilibrium occurring in the flashes and stripper/distillation column stages. In this regard, a comprehensive assessment of the accuracy of several equation of stages is reported in the recent paper by Sala et al. [36]. According to such analysis, the Peng Robinson equation of states with the calibrated binary interaction parameters found in [37] is the most accurate equation of states. For this reason, the CPU is modelled with the same equation of states.

3.2. Cycle modelling procedure

Fig. 3 shows the flowchart of the main activities performed in this work to obtain an accurate performance assessment of the cycle efficiency. For all the considered cases, the first step is a preliminary cycle simulation using the Aspen Plus models previously developed by Politecnico di Milano researchers and described in [12]. In the second step, the turbine, compressors and heat exchangers (recuperator, cooler and intercoolers) have been studied in detail to assess their performance, preliminary design and costs. Moreover, the CPU has been modelled in detail, differently from [12]. Both the cycle and CPU models run in Aspen Plus V10 [38].

The preliminary cycle simulation takes as input literature values

Table 2
Summary of the conditions at which the experimental data were available.

ID.	N1	O1	O2	A1	H1	H2	H3	NA1	NA2
Prop	Density	Density	Density	Density	Density	Density	Density	Density	Density
CO2	0.9585	0.9393	0.8709	0.9692	0.9000	0.9500	0.9800	0.9000	0.9500
N2	0.0415	–	–	–	–	–	–	0.05	0.04
O2	–	0.0607	0.1291	–	–	–	–	–	–
Ar	–	–	–	0.0308	–	–	–	0.05	0.01
H2O	–	–	–	–	0.1	0.05	0.02	–	–
Tmin [K]	303.22	303.22	303.22	303.22	348.13	323.14	323.14	323.14	323.12
Tmax [K]	383.14	383.14	383.14	383.14	498.11	498.11	498.11	423.20	423.26
Pmin [Mpa]	1.00	1.00	1.00	1.00	0.11	0.09	0.09	2.98	2.98
Pmax [Mpa]	20.00	20.00	20.00	20.01	10.24	8.89	9.27	30.95	30.95
n. exp point	97	100	100	100	63	75	75	75	75
Ref.	[33]	[33]	[33]	[33]	[34]	[34]	[34]	[35]	[35]

Table 3
Results of the validation procedure for the different EoS.

ID	N1	O1	O2	A1	H1	H2	H3	NA1	NA2	**AVG**
PENG-ROB	2.64 %	2.58 %	5.21 %	2.12 %	0.32 %	0.29 %	0.22 %	1.28 %	1.82 %	**1.71 %**
SRK	2.74 %	2.77 %	2.23 %	3.97 %	0.10 %	0.14 %	0.25 %	4.83 %	5.65 %	**2.32 %**
BWR-LS	2.80 %	2.69 %	4.42 %	1.76 %	0.09 %	0.12 %	0.09 %	0.86 %	1.06 %	**1.42 %**
LK-Plock	13.50 %	13.59 %	5.21 %	12.89 %	0.03 %	0.04 %	0.10 %	1.27 %	3.26 %	**5.01 %**
GERG2008	1.32 %	1.42 %	2.27 %	0.92 %	0.04 %	0.05 %	0.01 %	0.65 %	2.24 %	**0.90 %**

(reported in [11]) for the isentropic efficiency of the compressors and pressure drops of the heat exchangers. It computes a preliminary assessment of the composition, mass flow rates, pressures and temperatures of all the cycle streams.

These preliminary simulation outputs are used as inputs to perform the selection and preliminary design of the key cycle components, namely, the turbine, the heat exchangers and the compressors. Starting from the results of this preliminary simulation:

- The turbine is designed and simulated in "GS" (Gas Steam simulation code), a software for the simulation of gas turbine cycles developed by the Group of Energy Conversion Systems at Politecnico di Milano [25]. The results of the turbine design and simulation are then used to calibrate the cooled expander model of the Aspen Plus simulation.
- The heat exchangers of the recuperator, cooler and intercoolers are sized using literature heat transfer correlations. The resulting pressure drops and thermal losses are then assigned as input for the regenerator in the Aspen Plus model of the whole cycle.
- The type, diameter and rotational speed of each compressor are determined using the Balje diagram [39] and their isentropic efficiency estimated by correlations found in [40], a recent work on CO_2 compressors design optimization performed by Politecnico di Milano. The assessed compressor efficiency, together with the efficiency of the gearbox and electric drivers, are then included in the Aspen model of the cycle in order to perform the final cycle simulation.

As last step, the CPU is selected among the designs available in literature and simulated.

As far as the ASU is concerned, it was not modelled for sake of simplicity; the data regarding the specific consumption and the available heat from the aftercooler and main air compressor are taken from literature [1241], as will be detailed in section 3.2.

3.3. Main units modelling and assumptions

All the information about the modelling and assumptions made for the main cycle units is reported in this section. A more detailed preliminary design of the two main cycle units (Turbine and regenerator) was also performed in this study, with the double aim of providing better inputs for the Aspen Plus simulation, and a better sizing for the economic analysis. For this reason, they will be further discussed in Sections 3.4 and 3.5.**Regenerator model**

The regenerator is modelled in the Aspen Plus simulation as two multi-flow heat exchangers, which can properly deal with streams featuring variable heat capacity, connected in series. The temperatures of the hot streams exiting the high-temperature component are set equal to dew point temperature of the flue gases, while the temperature difference at the hot end is set equal to 20 °C. The temperatures of the hot flows at the cold end and the final temperature of the coolant sent to the turbine are then derived from the energy balances of the two blocks, while the temperature of cold flows exiting the low-temperature component is adjusted so as to obtain a minimum temperature difference of 5 °C. In order to prevent damaging to the turbine, the coolant temperature is set to be above 400 °C. These design criteria at the basis of the recuperator model allow using the heat available in the flue gases in the most efficient way, as shown in the cycle optimization work published [12]. The maximum pressure drops assumed for the regenerator on hot and cold sides, reported in Table 7, have been verified performing a preliminary sizing of the heat exchangers, as detailed in Section 3.4.

Finally, the maximum temperature of the exhaust gases allowed by the recuperator is assumed to be 725 °C, in agreement with the target value reported by the cycle developers in [7] for utility-scale full-size plants. It is important to notice that such high value is quite optimistic even for the material recommended by the cycle developers [8]. Indeed, to the best of our knowledge, the limited publicly available creep tests on diffusion bonded recuperators report that creep resistance starts to decay quickly at temperatures above 650 °C [42].**Combustor model**

The combustor is modelled as a complete conversion reactor performing the complete combustion of fuel species with a pressure drop of 3 bar (1 % of the inlet pressure). As for the oxidant stream, it is mixed with a fraction of the recycled CO_2 so as to obtain an oxidant stream (18 in Fig. 1) with an oxygen molar fraction equal to 13.34 $\%_{mol}$. Such dilution, as recommended in [2], is aimed at reducing oxidation/corrosion issues and hazards when heating up pure oxygen. An important assumption concerning the combustor is the excess of oxygen required to achieve CO conversion. According to [2,12], the minimum required excess of oxygen is 3 % compared to the stoichiometric value. Thus, the oxygen provided by the ASU is adjusted to meet such

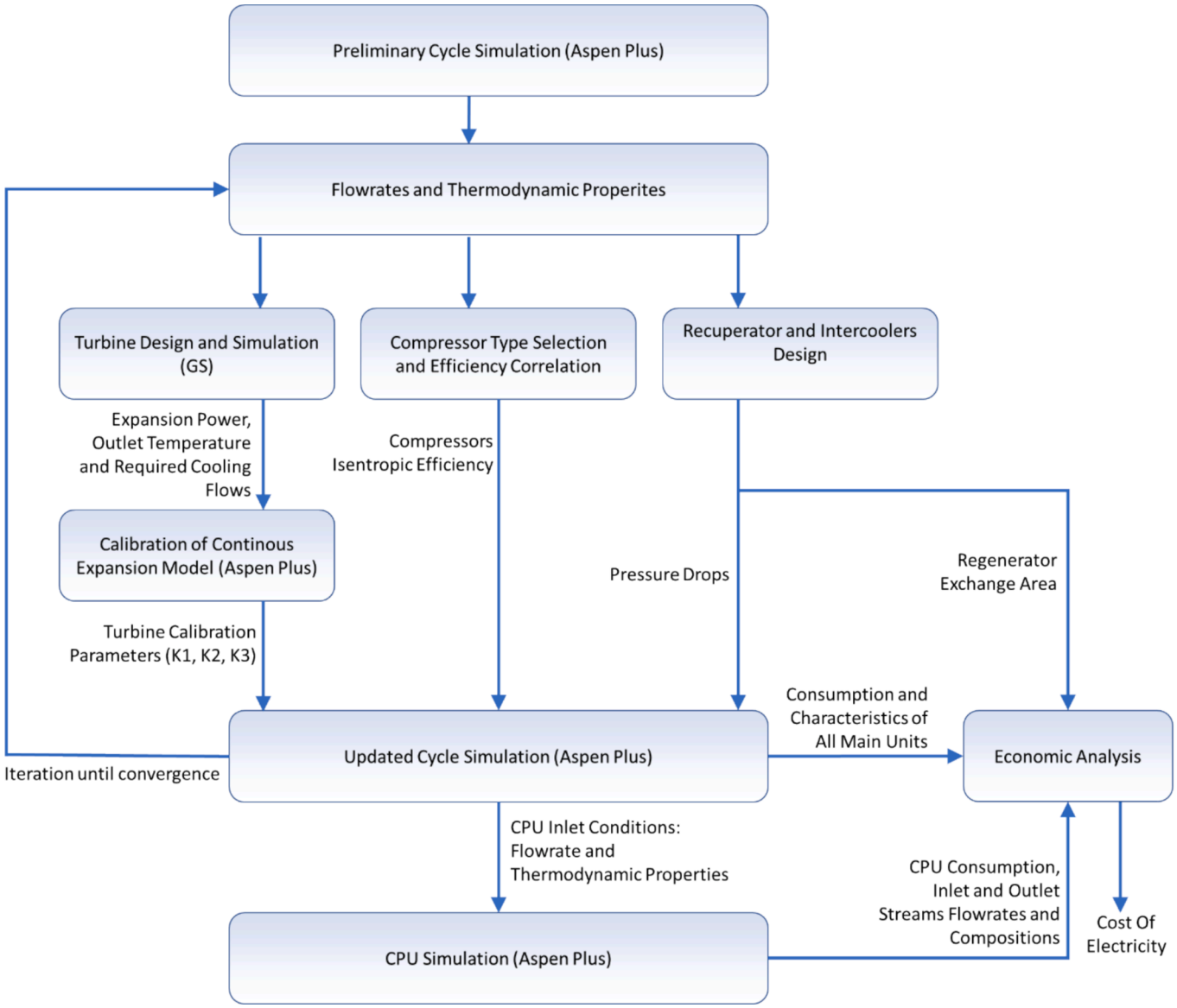

Fig. 3. Flowchart of the main activities performed in this work to simulate the cycle.

requirement. It is worth noting that higher excess values would have the triple disadvantage of increasing the ASU power consumption, diluting the captured CO_2 and increasing the power consumption of the recycle compressors of the Allam cycle.**Cooled turbine model**

For all cases except the 50 MW size (PS-50), a turbine featuring cooled blades is considered, with a technological level in agreement with a F-class gas turbine in terms of blade wall Nickel temperature (860 °C), thermal barrier coating thickness, convective and film cooling effectiveness [43]. For the 50 MW plant (PS-50), an uncooled turbine with a maximum allowed turbine inlet temperature of 950 °C is assumed, a value in line with uncooled micro gas turbines [44].

To model the cooled turbine in the cycle simulation, the continuous expansion model proposed in [12] was adopted. It is the 0-D simplified cooled turbine model also used for the IEA study [3] and all the subsequent studies on part-load [17 21]. It is a simplified model that can be easily integrated in the cycle simulation and optimization to assess the cooling flow requirement and calculate the power produced by the turbine without dealing with the details of the turbine design procedure (number of stages, blade geometry, velocity triangles, rotational speed, etc.).

In this model, the expansion is divided into multiple discrete steps (e.g., 15–20) and, for each step, the mass flow rates of required cooling flow is computed according to Eq. (1). The first n-1 steps are cooled, while the last one represents the uncooled portion of the expansion. All the cooled expansion steps are considered to have the same expansion ratio and isentropic efficiency. The expansion ratio of the cooled steps is adjusted to obtain the maximum imposed metal temperature at the inlet of the uncooled section.

$$m_{Ci} = K_1 \frac{(T_{Ii} - T_w)}{(T_w - T_{Ci})} W_{EXP-i} \quad (1)$$

where T_{Ii} is the inlet temperature of the gas entering the i-th expansion step, T_w the walls temperature, T_{Ci} the coolant temperature and W_{EXP-i} the power extracted from the expander at stage i, and K_1 is the main model calibration constant depending on:

- Flue gas composition, thermodynamic conditions (pressure and temperature), and velocity.
- Ratio between cross section area of the turbine and surface to be cooled.
- Loading factor of the stages

- Technology (convective cooling, film cooling, thermal barrier coating, etc.) and effectiveness of the cooling system.

The effect of cooling flow injection into the main flow is accounted as a pressure drop (Eq. (2) which increases with the ratio between the cooling flow mass flow rate m_{Ci} and the volumetric flow rate V_{Hi} of the hot flow.

$$p_{0i} - p_{li+1} = K_2\left(\frac{m_{Ci}}{V_{Hi}}\right)^{K3} \quad (2)$$

The values of the parameters K_1, K_2, K_3 have been calibrated using the 1-D turbine model described in Section 3.3.Once the 1-D preliminary design of the turbine is computed, the value of the main parameter K1 is set to match the overall cooling flow requirement calculated in the preliminary design, while K2 and K3 are kept equal to [12] The results of the calibration are reported in Table 4.

As far as the cooling flow temperature is concerned, it is important to note that the cooling flows are pre-heated in the recuperator using the excess heat not recovered by the moderator and oxidant flows. The resulting cooling flow temperatures vary between 110 °C and 405 °C throughout the different analyzed cases. It is worth noting that low values of this temperature may lead to excessive thermal stresses in the turbine blades and a thorough thermo-mechanical analysis of the turbine blades should be performed to assess the minimum required temperature. Such an analysis will be the objective of future studies.

As for the turbine gearbox (needed for the cases with non-synchronous turbine, i.e., PS-200, PS-100 and PS-50) and the electric generator, the following values and sources are considered:

- According to the Baker Hughes website [45], large size gearboxes (with power ranging from 500 kW to 37 MW) feature a mechanical efficiency close to 99 %. Larger gearboxes may reach higher mechanical efficiency but no data has been found in the literature.
- The electric efficiency of generators is taken from the Siemens website: 99 % for large generators (370–560 MVA) and 98.5 % for medium large (25–370 MVA) [46].

Compressor model

As far as compressors are concerned, the Aspen model uses the basic compressor block with specified isentropic efficiency, mechanical efficiency and electrical efficiency of the driver. The starting pressure of the dense phase compression is adjusted so as to have a density above 645 kg/m^3 (corresponding to the supercritical conditions density) at the inlet of the dense-phase compressor. Due to the presence of incondensable gases, this pressure value varies as a function of the purity of the oxygen stream provided by the ASU, as detailed in Section 6.2 concerning the sensitivity analysis on oxygen purity.

The isentropic, mechanical and electrical efficiency values of the compressors are taken from literature correlations as functions of the plant size and pressure ratio. In particular, for each compressor of each plant considered in this study, the preliminary sizing is performed using the Balje diagram [39] with the aim of determining the optimal type (radial vs. axial flow) and optimal rotational speed (information useful to assess the requirement of adopting a gearbox). The preliminary sizing showed that all the compressors are single stage and radial. The isentropic efficiencies of compressors have been evaluated as a function of the size parameter (SP) expressed in [m] and pressure ratio with the best-fit curve reported in [40] valid for CO_2 compressors. The correlation uses as input parameter the size parameter of the compressor (SP), defined in Eq. (3).

$$SP = \frac{\dot{V}^{0.5}}{\Delta h_{IS}^{0.25}} \quad (3)$$

where V is the volume flow rate at the compressor inlet and Δh_{IS} is the isentropic enthalpy drop (ideal specific work) of the single compressor stage, the parameter usually adopted to account for scale effects on turbomachinery efficiency. For size parameters lower than 0.08 m, the isentropic efficiency is taken from the correlation published in [40]:

$$\eta_{IS} = 0.4649 \cdot SP^{0.8033} - 0.0183 \cdot \beta^{0.8870} + 0.8298 \quad (4)$$

where β is the compressor pressure ratio. For SP > 0.08 m, the correlation has been extended by considering the following logarithmic function of the size parameter:

$$\eta_{IS} = 0.92847 + 0.071534 \cdot log_{10}(SP) \quad (5)$$

This function has been devised to match the efficiency curve reported in [40] at SP = 0.08 m and to have a value of 90 % at SP ≥ 0.40 m. The plot of the correlation over the whole range of SP is shown in Fig. 4.

The efficiency of large size industrial electric motors is assumed to vary in the range 98.2 %-98.6 % (values taken from [47] for different sizes) with a logarithmic law of the shaft power:

$$\eta_{EL} = 0.982 + 0.4292 \cdot log_{10}(P_{SH}) \quad (6)$$

where P_{SH} [MW] is the shaft power. As for gear-boxes, we assume a mechanical efficiency of 99 %, according to [45].**CO2 purification unit (CPU)**

In this work, among the available CPU process configurations, the "high recovery" distillation-based scheme (patented by Air Products [48] and then studied by Strube and Manfrida [49]) is selected because of its considerably high recovery rate (i.e., the fraction of inlet CO_2 which is released as high purity stream) approaching 99 %. The scheme is reported in Fig. 5. The key idea is to improve the CO_2 recovery (i.e., reducing the fraction of CO_2 contained in the vent gas) by recycling the gas flow leaving the top of the distillation column and cooling it down to low temperature to condense and recover more CO_2. In this configuration the CO_2 rich flue gas stream resulting from oxy-combustion, after being compressed to 35 bar (optimal CPU pressure according to preliminary simulations) and dehydrated moves to a multi-flow heat exchanger. After passing through the heat exchanger for the first time the stream provides heat to the reboiler of the stripper, where liquified CO_2 is being purified. This stream is further cooled down (in between −44 °C and −48 °C) and sent to the flash drum separator. The gas stream contains mostly incondensable gases and is vented to the atmosphere (after optional preheating and expansion to recover some electric power). The liquid stream of the separator is then throttled to 15–18 bar and fed to the stripper column. The gaseous stream leaving the top of the stripper is recompressed and recycled to the inlet flow. The liquid stream leaving the bottom of the stripper is divided into two parts which are then throttled to 7 and 14.5 bar respectively, to match the temperature – heat duty profile inside the multi-flow HX. The addition of a flash separator operating at a temperature lower than that at the stripper inlet reduces the flow rate of vented CO_2, resulting in a net CO_2 capture efficiency in the range 93–98 % (depending on the inlet composition), appreciably higher than that achievable with standard distillation-based CPU schemes.

As mentioned in the first paragraph of Section 3, the CPU has been modelled in Aspen plus [38], employing the Peng-Robinson equation of state: the choice of this particular equation of states is based on the accuracy evaluations performed in our recent work [50,36].

Table 4
Values of the parameters K1, K2 and K3 for different plant sizes.

Net Plant electric power output	400 MW (BC)	300 MW (PS-300)	200 MW (PS-200)	100 MW (PS-100)
K_1	1.14135x10^{-6}	1.644x10^{-6}	1.0x10^{-6}	0.86x10^{-6}
K_2	0.75	0.75	0.75	0.75
K_3	1.031734	1.031734	1.031734	1.031734

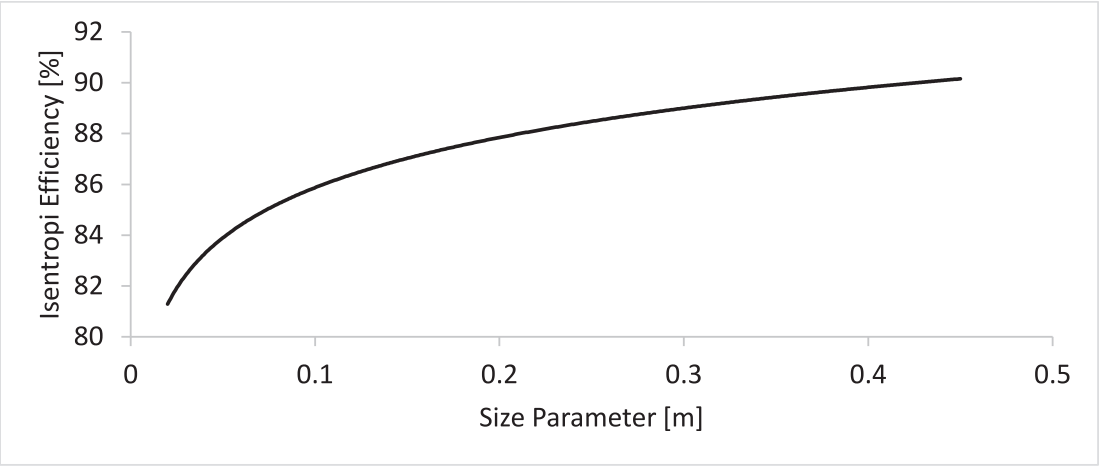

Fig. 4. Plot of the CO2 compressors isentropic efficiency as a function of the SP.

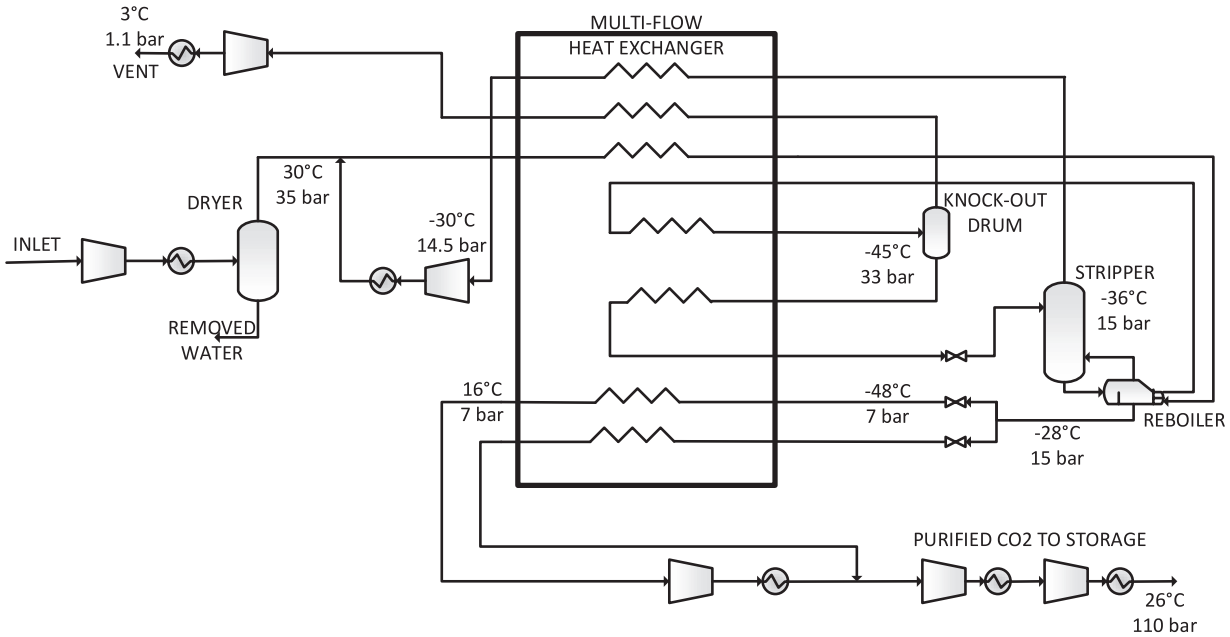

Fig. 5. Flowsheet of high recovery stripping/distillation-based CPU proposed in [48] and modified to receive high pressure CO_2 (at 29.1 bar) from the Allam cycle.

Our preliminary simulations indicate that it is possible to achieve very low levels of oxygen in the captured CO_2 stream (i.e., O_2 concentrations can be kept below 10 ppm) by adjusting the operating and design variables of the process (pressures, temperatures, mass flow rates, distillation column design parameters), a value that would allow to avoid the corrosion issues generated by the presence of oxygen in the highly pressurized CO_2 stream to be transported and stored. For this purpose, all of the simulations performed with the presented CPU have a CO_2 purity above 99.99 % in the stream to storage, and an O_2 concentration below 10 ppm (molar basis). Fig. 5 reports also the key design pressures and temperatures of the process.**Air separation unit**

The Allam cycle receives high purity oxygen from an air separation unit (ASU). Cryogenic air separation units represent the current reference technology to produce high amounts (tons per day) of oxygen and are widely used in the chemical and iron and steel industries. The largest commercial plants have capacities exceeding 5,000 metric tons per day per single line [51,52], a flow rate large enough to supply a 400 MW Allam cycle.

The study performed in [53] pointed out how ASU configurations more complex than the traditional dual column plant can reduce the energy consumption for air separation at the expense of an increase in investment cost. Since the energy required for air separation increases with the purity of the oxygen produced, from the plant efficiency perspective, the purity of the oxygen supplied to an oxyfuel power cycle should be set to a value whereby the energy savings in the CPU that removes impurities no longer compensates the additional consumption of the ASU for a further increase in purity. To achieve purity above about 97 % an additional rectification column is required to separate oxygen and argon [54] resulting in a higher capital cost which may be unjustified in the absence of an adequate demand from an adjacent argon market.

Simulation of the whole ASU was not considered necessary in the frame of this study because, for the integration with the Allam cycle, it is sufficient to know the electric power consumption and the heat duty (along with the temperature level) that the ASU can supply to the Allam cycle. For this purpose, [41] provides the specific electric power consumption per kg of produced oxygen as a function of oxygen purity and delivery pressure. Three different purity levels are considered in the present study for the sensitivity analysis on oxygen purity: 95, 97 and

99.5 %. The respective specific consumptions are reported in Table 5. As for the assessment of the heat recovered from the main air compressor aftercooler, we modelled the main air compressor and its aftercooler assuming a pressure ratio of 7.5, a compressor polytropic efficiency of 85 %, a mechanical efficiency of 98 % and a temperature difference of 20 °C between the air and the hot thermal oil (a loop of hot thermal oil was assumed to be used to deliver the heat from the ASU to the regenerator). This calculation assessed that the ASU can supply a heat duty of 1015.1 kJ/kg_{O2} to the recuperator of the Allam cycle via a diathermic oil loop operating in the temperature range from 75 to 255 °C.**Other assumptions, basis of design**

The Allam cycle and the rest of the plant (ASU and CPU) are designed assuming the following basis of design:

- Cooling water is available at the plant site at 21 °C (yearly average temperature) and it allows cooling the cycle streams to 26 °C.
- The natural gas composition is reported in Table 6 (same considered by Scaccabarozzi et al. [12]).

Summary of main assumptions and design criteria

The summary of the key modelling assumptions adopted for all the considered cases is reported in Table 7.

For each case (BC, PS-300, etc.), the cycle is designed according to the following main design criteria:

- The oxygen flow rate is adjusted to meet the minimum required excess of oxygen in combustion;
- The moderator flow rate is adjusted to achieve the maximum allowed turbine outlet temperature of 725 °C
- The turbine outlet pressure is optimized to maximize the net plant electric efficiency (Allam cycle + ASU + CPU).

3.4. Preliminary turbine design and performance assessment (GS)

As shown in [12], the Allam cycle features a maximum efficiency with a turbine inlet temperature in the range 1100 °C-1200 °C which requires a cooling systems for the blades and case [5]. Unfortunately modelling a cooled turbine is a complex task since it calls for the calculation of the required cooling flows and efficiency loss due to the injection of the cooling flows into the main hot flow (see, e.g., Horlock [55]). The software Aspen Plus, originally developed for chemical processes, does not feature such a complex expansion model. For this reason, it is necessary to perform a preliminary design of the expander (because the requirement of cooling flows depends on the turbine geometry, number of stages, stage loads, etc.) and adopt codes which were developed specifically for modelling cooled gas turbines, such as [56,57,58]. In this work we used "GS" (Gas Steam simulation code), a software for the simulation of gas turbine cycles developed by the Group of Energy Conversion Systems at Politecnico di Milano (published in [59]). Then, the results of the preliminary turbine design have been used to calibrate the simplified cooled turbine model developed by Scaccabarozzi et al. [58] and used in Allam cycle model (Aspen Plus).

In detail, the GS software features a 1-D model which is able to perform the preliminary design of the turbine (number of stages, mean diameter of each stage, reaction degree and load coefficient of each stage, isentropic efficiency of each stage, etc.) and determine the cooling flow requirement of each blade row (stator, rotor, etc.). The model considers validated literature correlations to model the heat transfer between hot fluid and blade as well as blade wall and internal cooling flow, and the friction losses induced by film cooling and the injection of cooling flows into the main stream. The required key inputs are the number of stages, the rotational speed, the stage reaction degree and load coefficient, mean diameter and flow coefficients at inlet and outlet, the maximum blade metal temperature, and the thickness of the thermal barrier coating. Full details are reported in [25] and omitted here for the sake of space. The model has been validated on several commercially available gas turbines as reported in [43,59]. On the other hand, due to the lack of experimental data on cooled supercritical CO_2 turbines (to the best of our knowledge, there is only one cooled supercritical CO_2 turbine currently installed at the Demonstration plant in Texas [10] but the data are not publicly available), it was not possible to validate the GS turbine model at the relevant conditions of the Allam cycle turbine. Thus, in order to double check the validity of the GS model for a cooled supercritical CO_2 turbine in absence of publicly available data, the only possible actions were:

- Check the validity of the correlations adopted for the transport properties (thermal conductivity [30], viscosity [31]) at the relevant Allam cycle conditions CO_2.
- Check the accuracy of the efficiency correlations adopted in GS against the results of the more detailed 1-D model recently published by Dipierro et al. [60] for supercritical CO_2 turbines.

Table 5
Summary of the specific electric power consumption and medium temperature heat (range 255 °C – 75 °C) recoverable from the ASU according to [41].

	99.5 % purity @ 120 bar	97 % purity, @ 120 bar	95 % purity, @ 120 bar
ASU specific el. power consumption [kJ_{el}/kgO_2], [26]	1390	1320	1310
ASU specific heat recovered from the main air compressor aftercooler [kJ_{th}/kgO_2]	1015	1015	1015

Table 6
NG Composition.

Natural gas analysis, $\%_{mol}$	
CH_4	89
C_2H_6	7
C_3H_8	1
C_4H_{10}	0.10
C_5H_{12}	0.01
CO_2	2
N_2	0.89
Total	100
Lower heating value (MJ/kg)	46502
Temperature (°C)	15
Pressure (bar)	30

Table 7
Summary of the main assumptions adopted for the preliminary cycle simulation. The numbers are referred to Fig. 1.

	Unit	Value
Maximum allowed turbine outlet temperature (T_8)	°C	725
Maximum Metal (Nickel superalloy) Temperature of turbine blades	°C	860
Turbine inlet pressure (p_6)	bar	306.95
Turbine outlet pressure (p_8)	bar	optimized
Hot Side REG Temperature Approach (T_8-$T_{4\text{-}5}$)	°C	20
Minimum Internal REG Temperature Approach	°C	5
Heat transfer ΔT between ASU Air and Oil Loop	°C	20
Pressure ratio of ASU Main Air Compressor	–	7.5
Hot Oil Delivery Temperature (T_{20})	°C	255
Oxidant O_2 Molar Fraction (flow 18)	%	13.34
O_2 percentage excess of combustion	%	3
Regen. High Pressure Flows Inlet Pressure ($p_{14\text{-}15\text{-}19}$)	bar	311.6
Regen. Low Pressure Flows Inlet Pressure (p_8)	bar	30.6
Combustor Inlet Pressure (p_3)	bar	310.0
Regen. High Pressure Flows Pressure Drop	bar	1.6
Regen. Low Pressure Flows Pressure Drop	bar	0.8
Combustor Pressure Drop	%	1.0
Condenser and Intercoolers Pressure Drop	bar	0.4–2.4

The key common design criteria adopted for the cooled turbines for the 400 MW, 300 MW, 200 MW and 100 MW plants are summarized below:

- Maximum metal allowed blade metal temperature: 860 °C.
- TBC thickness: 250 μm.
- Adoption of film cooling.
- Front loaded expander: reaction degree increasing linearly from zero (impulse stage at inlet) to 0.30.
- Rotational speed: synchronous for the 400 MW and 300 MW plants and optimized for the other smaller sizes (200 MW, 100 MW, 50 MW), for which the existence of suitable gear boxes was assumed. The largest size plants must feature a synchronous turbine since, to the best of our knowledge, there are no gear boxes available on the market for their power range. According to [61] and [62], the largest gearboxes available on the market today reach a size of 180 MW.
- Mean diameter of the first stage is determined so as to have a ratio blade height/mean diameter equal or greater than 0.04. Lower values should be avoided due to the excessive end-wall and tip clearance losses occurring for blades with low aspect ratio [63 29].
- The mean diameter increases by 1.2 % for each row (stator and rotor).
- The number of stages is adjusted in order to reach the target outlet static pressure. The lower is the mean diameter of the turbine and the more stages are required, as indicated also in [64].

As for the case of 50 MW plant size, given the relatively small size, we considered an uncooled axial turbine with optimized rotational speed (due to the availability of gear boxes for such size). Stages are front loaded also in this case in order to limit the requirement of high temperature materials.

Table 8 summarizes the results of the preliminary turbine design performed with the GS software.

Owing to the relatively low rotational speed and particularly dense inlet fluid, the larger size turbines for the 400 and 300 MW plants suffers from relatively small blades in the first turbine stage. Thus, to avoid excessive end-wall and tip losses in the first turbine stages, the mean diameter of the first turbine stage is set so as to have a ratio blade height/mean diameter of 0.04. The effectiveness of this design criteria has been confirmed by the results of recent publication investigating the optimal design of the Allam cycle turbine [58]. It is important to note that the resulting mean diameter is half that of a gas turbine of the same power output. The main consequence is the limited peripheral velocity (< 200 m/s) and work which can be extracted by each stage, which has the direct effect of making the large turbines require respectively 6 and 8 stages, and the first 5 need to be cooled. In particular, the design of the 300 MW plant turbine results particularly penalized by the lack of gearboxes and the impossibility of adopting higher rotational speeds, as it is highlighted by the number of required stages. For this reason, in this study, it was decided to assume that the 200 MW plant turbine can be equipped with a gearbox (even if its gross power output, 304.5 MW, is above the range of currently available gearboxes).

The plants with ≤ 200 MW net power output can adopt an optimized rotational speed to keep the ratio blade height/mean diameter within the optimal range (0.06–0.01), without limiting the turbine mean diameter. This allows reaching higher peripheral speeds and work extracted per stage, with the main advantage of requiring only 5 stages (of which 4 are cooled).

It is important to notice that the work extracted per stage is not only important when determining the number of turbine stages but also influences the specific requirement of cooling flows. In fact, the higher is the stage load, the lower is the specific requirement of cooling flow expressed in kg/s per unit of power extracted or ratio between cooling flow rate and inlet hot mass flow rate (assessed considering a reference cooling flow inlet temperature). For instance, the 100 MW and 200 MW turbine require a cooling flow rate which is only 7 % of turbine inlet flow while the 300 MW design require the double amount (approx. 14 %). Such larger cooling flow requirement has two negative effects on the total cycle efficiency:

- The cooling flow injection into the main expanding flow causes fluid-dynamic losses which penalize the turbine isentropic efficiency.
- The turbine cooling flows follow a thermodynamic cycle (compression preheating in recuperator, heating up in the turbine blades and mixing process with the hot turbine flow, expansion) featuring a lower efficiency than the flow going to the combustor due to the high pressure drops in the blade channels and limited maximum cycle temperatures.

3.5. Regenerator preliminary design

In order to determine the pressure drops caused by the regenerator and assess its size and capital cost, it is required to divide it into multiple interconnected heat exchangers (featuring one hot stream and one cold stream). Indeed, the regenerator of the demonstration plant shown in ref. [7] consists of a network of heat exchangers (HXs), where different materials and designs can be adopted for each HX. The need of adopting different materials and designs in each HX is caused by the large variation of temperature (from 50 °C to above 700 °C) and volumetric flow rates of the hot and cold flows. Thus, to perform the preliminary design of the regenerator, the multi-flow heat exchanger adopted in the Aspen Plus model has been converted into a network of HXs (a so called “heat exchanger network”, HEN). The HEN has been derived taking as reference the design of the recuperator for the demonstration Allam cycle plant reported in [7] and by adding the heat exchangers between the hot oil loop of the ASU and the moderator recycle flow. The resulting HEN comprises 12 basic heat exchangers arranged as shown in in Fig. 6. It is important to notice that such HEN meets the Pinch Analysis design rules [65], i.e., it is optimal from the point of view of energy efficiency and it allows recovering the same heat as the multi-flow heat exchanger of the Aspen Plus model.

The heat exchangers of the HEN are divided into four temperature sections, identified in Fig. 6 as HT, MT, LT and LLT, starting from the hottest one in order of decreasing temperature. The heat exchangers in the HT section (containing HXs 1 and 2) are made in Inconel 617 and feature hot flows temperatures from 550 °C to 725 °C. The HXs in the MT

Table 8
Main results of the preliminary turbine design performed using the GS software.

Turbine power	MW	661.43	469.25	301.74	150.38	60.99
Net power	MW	400	300	200	100	50
TIT	°C	1162	1162	1211	1202	900
TOT	°C	717.6	708.4	735.6	734.4	575.6
TIP	bar	307	307	307	307	307
TOP	bar	30	30	30	30	30
m_{IN}	kg/s	1200	900	540	273	205
T_{MET}	°C	860	860	860	860	900
Rot. Speed	rpm	3000	3000	8000	11300	18000
$D_{M,1st}$-$D_{M,last}$	[m]	1.26–1.73	1.15–1.36	0.55–0.72	0.39 – 0.51	0.25 – 0.31
U_{1st}	[m/s]	198	181	231	231	234
N_{ST}	–	6 (5 cool)	8 (5 cool)	5 (4 cool)	5 (4 cool)	4
m_C/m_{IN}	–	0.0762	0.1413	0.0738	0.077	0
Isen. Eff.	%	89.00*	89.00*	88.50*	88.00*	89.00
Mech eff.	%	99.86	99.86	99.00	99.00	99.00
El. Eff.	%	99.00	99.00	98.50	98.50	98.50

* For the cooled turbines, the table reports the isentropic efficiency of the discretized expansion steps of the continuous expansion model. Due to the recovery effect, it is not directly comparable with the isentropic efficiency (from inlet to outlet) of the cooled turbine but it can be considered as a quantitative index of the expansion efficiency of the turbine.

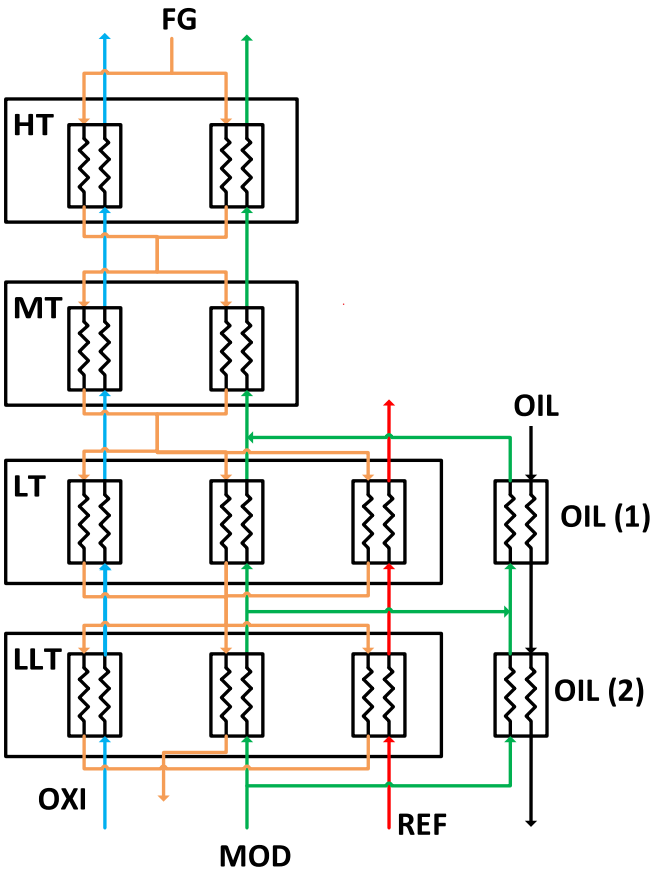

Fig. 6. Internal arrangement of the recuperator designed for the Allam cycle.

section cover a temperature interval from 248 °C (temperature of the inlet diathermal oil used for the ASU thermal integration) to 550 °C, upper limit for high grade steels, like SS316, typically adopted for the recuperators of sCO_2 cycles [66]. The boundary between the LT section and the LLT section is the water dew point (109 °C) at design conditions: in the LLT section a fraction of the water in the exhaust gases condensates increasing the risk of corrosion and, on the other hand, providing additional latent heat. For this reason, compared to the LT section, the HXs in the LLT section requires a different partition of the exhaust gases among the three HXs (8, 9 and 10) and, probably, a different type of corrosion-resistant material. To model the additional preheating of the cold streams due to the heat integration with the ASU it is necessary to consider two heat exchangers (HX 11 and 12), where a fraction of the cold flows is heated (either the moderator or the oxidant, the effect on the cycle efficiency would be equivalent) using the heat recovered from the ASU. As indicated in Section 3.2, it is considered to adopt a loop of thermal oil to transfer this heat from the air aftercooler of the main air compressor to the Allam cycle. For safety reason, it is considered to supply the heat from ASU to a fraction of the moderator and not to the oxidant, since thermal oil is flammable.

As far as the detailed regenerator design, the following methodology is applied. Each heat exchanger is considered to feature a cross-flow arrangement, according to the Heatric heat exchanger picture shown in [67]. Moreover, the flue gases are considered to have a single passage in order to limit their pressure drops, while the cold streams may have multiple passages. It is important to notice that the reason behind such choice lies in the fact that the pressure drops on the exhaust gases side are more critical than those on the cold streams (oxidant and moderator) side, because the volumetric flow rate of exhaust gases is 46 times that of the cold streams: one mbar of pressure drop on the exhaust gases would entail an expansion power loss of about 7 kW (approx. equal to the volumetric flow rate multiplied by the pressure drop and the polytropic expansion efficiency of the turbine); while one mbar of pressure drop on the side of the oxidant and moderator can be compensated by raising by one mbar the outlet pressure of the dense-phase compressor with an increase in power consumption of only 0.2 kW (approx. equal to the volumetric flow rate multiplied by the pressure drop and divided by the polytropic expansion efficiency of the compressor).

Fig. 7 shows a schematic view of the HT regenerator section. The heat exchangers is considered to be a diffusion bonded compact heat exchanger [66], where the hot flue gases flow in the horizontal direction and the cold flows may have multiple passes in the vertical direction (with reference to Fig. 7). The basic constructive unit assumed in this study for the heat exchangers is shown in the right section of Fig. 7: the channels where the exchanging fluids flow are carved on the two sides of plates that are then divided by a separator.

The number of vertical and horizontal channels as well as the number of passages has been determined to achieve the desired transfer of thermal power. They are found in order to meet the following design specifications:

1) For the channels a rectangular shape with a height of 10 mm and a width of 3.5 mm is assumed, with a wall thickness of 1.6 mm.
2) The exhaust gas velocity must be below 10 m/s.
3) The dense-phase fluids must have a velocity below 5 m/s.
4) The distributed pressure drops for the overall recuperator must not exceed those assumed in the process simulation: 0.8 bar for the exhaust gases and 1.6 bar for the moderator and oxidant flow (concentrated pressure drops due to U-turns on the dense-phase fluid and headers are neglected).
5) The transferred heat matches the design requirement specifications. The heat transfer coefficients are determined with the Dittus-Boelter correlation for forced convection into channels [68]. It is considered to enhance the heat transfer by using semicircular ribs on the bottom of the channels using the correlations in [69]. According to preliminary analysis, the ribs allow decreasing the heat transfer area by a factor of 30 % while meeting the limits on the pressure drops.
6) In each section (HT, MT, LT and LLT), the heat exchanger between flue gas and moderator and the heat exchanger between flue gas and oxidant are arranged in parallel, as shown in Fig. 6. This way, the two HXs have the same dimension and number of channels both in height and length and similar pressure drops on the flue gas side, therefore thy can be coupled as shown in Fig. 7.

The design problem obtained from the indicated procedure can be written as an optimization problem, where the optimization variables are the number of horizontal and vertical channels in each plate, the number of platers in each heat exchanger and the number of passages of the flow (set to 1 for the hot flows, to reduce the losses on the hot side). The adopted heat correlations make the problem strongly non-linear; therefore the obtained formulation is a Mixed-Integer Non-Linear Programming Problem (MINLP), which is solved with the objective of minimizing the overall heat exchanger volume. The problem is written using the Python-based optimization modelling language Pyomo [70], with Baron [71] as external solver.

The main results of the heat exchangers sizing procedure are reported in Table 9, where:

- Nh, Nb and Nd are the number of channels in the H, B and D dimensions, and the numbers (1, 2, 3) refer to the oxidant, moderator and turbine cooling sections of the regenerator, respectively.
- H, W and D are the overall section dimensions, as in Fig. 7.
- N cold pass is the number of passages of the cold flow in the corresponding section.

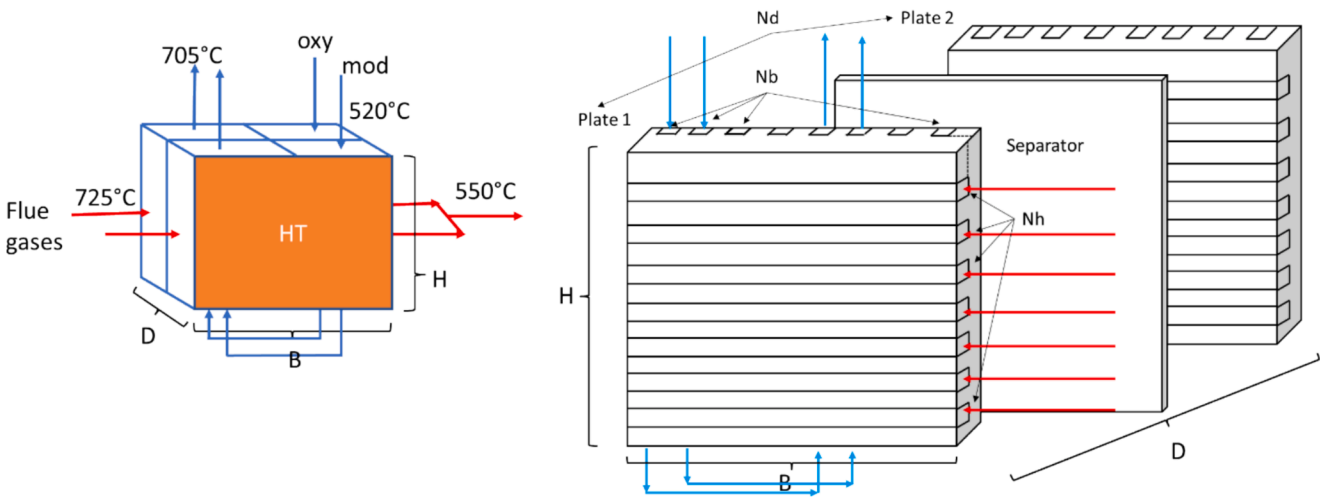

Fig. 7. Schematic view of the HT section of the heat exchanger and plate channels arrangement.

4. Economic analysis assumptions and methodology

4.1. Economic analysis assumptions and cost models

In order to evaluate the economic potential of the cycle, a preliminary economic analysis has been performed considering the 400 MW Allam cycle base case and comparing it with a reference NGCC with post-combustion capture.

The following cost models have been used to assess the bare module costs (equipment cost at the vendor's gates) of the main cycle equipment units:

- For the ASU, CPU, and Balance of Plant the cost estimate reported in [2] is considered, scaled for different units' sizes using scale factors derived from literature studies and industrial projects. The details of the cost functions are reported in Table 10.
- For the turbine, an average cost between a steam turbine and a gas turbine of the same size is assumed.
- For the CO_2 compressors, the cost correlation published in [72] are adopted.
- For heat exchangers, the cost correlation published in [73] and based on data gathered from engineering and procurement companies are used.
- For the recuperator, performing the detailed sizing of the single diffusion-bonded compact heat exchangers shown in Section 3.3 allows to derive the overall exchanger size and heat transfer surface. The cost function used to determine the cost is derived from the data published in the Heatric's white paper [66], reporting a target cost of 25 \$/kW_{th} for the recuperator of closed loop sCO_2 cycles (using stainless steel 316). From the published data the specific cost per unit of heat transfer area and the scale factor were back-calculated (the values are reported in Table 10). For the high temperature section of the recuperator (temperature above 550 °C), Inconel 617 is assumed as construction material, in accordance with the inventors recommendations [7]. For this section, a cost factor increase of 5 is considered (i.e., 5 times more expensive than SS316).

4.2. Economic analysis methodology

The economic analysis of each considered cycle has been structured following the methodology adopted by Amec Foster Wheeler in [2]. The steps of the methodology are detailed in the following:

a) Total Plant Cost (TPC) estimate: $TPC = F\ x\ TEC$

Where TEC denotes the Total Equipment Cost and F accounts for the additional Installation costs and Contingencies. In agreement with what considered in [2] $F = 2$ is assumed for all technologies. These additional costs are assumed to be 65 % Construction and other costs, 16 % Engineering and Procurement Services, 19 % Contingencies.

b) Total Capital Requirement (TCR) estimate: $TCR = G\ x\ TEC$

Where $G = 1.3$ (according to [2]), and it accounts for 8 % interest rate during construction, Spare parts cost (assumed as 0.5 % of TPC), start-Up cost (2 % of TPC + 25 % of fuel cost for one month, + 3O&M months and 1 month of chemicals/catalyst), Owner's cost (7 % of TPC).

c) Fixed Operating and maintenance costs:
d) Labor cost: since [7] estimated to need 82 persons (with a cost of 60,000 €/year each) for a power plant with two 400 MW trains, 75 % of such personnel is assumed to be needed for a single train.
e) Maintenance cost: assumed to be 2,5%/year of TPC for novel technologies (cooled turbine and recuperator), 1,5%/year of TPC for conventional ones (rest of plant). A Ratio labor-materials of 40–60 is assumed.
f) Overhead charges: management, administration etc.: 30 % of operating labor and maintenance
g) Insurance and local taxes cost: 0.5 % of TPC
h) Variable Costs:
i) Natural Gas cost ranging from 6 to 30 €/GJ (LHV), with a base case of 12 €/GJ (average value of TTF cost in 2021 [74]).
j) Full-load operation for 7884 h/y (90 % capacity factor)
k) Chemicals cost: same specific assumption as [2], corresponding to 0.06 €/MWth
l) Carbon Tax on CO_2 emissions (CO_2 vented from CPU): 85 €/t, average of the carbon cost in the European Union Emission Trading Scheme (EU ETS) in 2022 [75]
m) Cost for CO_2 transport and storage assumed to be equal to 20 €/t, average between the base case and the rapid cost decrease scenario for Europe in [76]
n) Other relevant economic assumptions:
o) The Chemical Engineering's Plant Cost Index (CEPCI) is adopted to actualize to 2022 the cost of all the cycle components [77].
p) \$/€ Conversion Rate = 1.15: it is the average of the exchange rate from 2014 (assumed in [12], used as a reference for the methodology and most of the costs) and 2022. It is required to convert the capital cost data of compressors, recuperator and all the components expressed in \$ into €.

Table 9
Main results of the regenerator sizing procedure.

	u.m.	HT	MT	LT	LLT	OIL LT	OIL LLT
Heat Exchanged	MW	285	234	108	134	37	14
Average Heat Transfer Coefficient	W/ m^2K	763	648	596	420	847	967
Number of horizontal channel rows, Nh		349	400	350	300	271	151
Number of vertical channel rows, Nb		223	394	500	582	293	300
Number of plates of HX between exhaust gases and oxidant, Nd1		300	300	350	300	–	–
Number of channels of HX between exhaust gases and moderator, Nd2		286	291	240	312	–	–
Number of channels of HX between exhaust gases and turbine coolant, Nd3		–	–	3	64	–	–
Number of channels of HX between oil and moderator		–	–	–	–	270	210
Number of passes on cold side		2	3	4	4	15	15
Number of passes on hot side		1	1	1	1	6	10
Height of the HX section, H	m	4.05	4.64	4.06	3.48	2.33	1.30
Width of the HX section, W	m	2.59	4.57	5.80	6.75	2.52	2.58
Size of the HX section between exhaust and oxidant, D1	m	3.06	3.06	3.57	3.06	–	–
Size of the HX section between exhaust and moderator, D2	m	2.92	2.97	2.45	3.18	–	–
Size of the HX section between exhaust and turbine coolant, D3	m	0	0	0.03	0.65	–	–
Size of the HX section between oil and moderator	m	0	0	0	0	2.75	2.14
Total HX heat transfer surface	m^2	14284	21779	32502	36967	3872	1718
Total volume of HX	m^3	63	95	142	162	16	7
Total mass of the HX	ton	210	429	486	565	63	29

q) Discount rate 8 %, 25 years of useful life, 12 years depreciation, 3 years construction, corresponding to a Capital Carrying Charge rate of $CCR = 9.37$ %.

4.3. Comparison with NGCC with Post-Combustion CCS

As an additional benchmark technology, the economic analysis of a F-class 650 MW NGCC with post-combustion CO_2 capture system studied in the 2019 NETL report [3] was considered, featuring a net electric efficiency of 52.8 % (carbon capture and storage included). The plant relies on the CANSOLV CO_2 absorption system and the cited report details performance, capital and operating costs. Starting from these cost and performance estimates, we updated the fuel cost, the CO_2 transport costs and the CO_2 emission costs using the assumptions of this study for comparison purposes.

5. Base case results and discussion: 400 MW Allam cycle design

The considered base case features a 400 MW Allam cycle, considering a 99.5 % purity ASU and achieving a net electric efficiency of 53.13 % (ASU and CPU included). All the cycle assumptions and models adopted in this base case are the ones reported in Section 3. The main numerical results are reported in Table 11.

Even though the base case shares the same size and most modelling assumptions as the plant previously optimized by Scaccabarozzi et al. [12], the efficiency computed in this work is about 1.2 percentage points lower (53.17 % vs. 54.43 % of [12]). A detailed comparison of the two cycles was performed, showing how such a difference in efficiency is mainly due to the following two reasons:

- This work considers a lower temperature level of the heat supplied by the ASU to the regenerator (−20 °C, due to the use of thermal oil employed for the heat transfer). This causes an efficiency drop of about 0.4 percentage points.
- In this work also the additional power consumption of the CPU is included (which was not modelled in [12]), causing a loss of about 0.6 percentage points.
- A different equation o states is adopted in the present study: [12] employed the Peng-Robinson EoS, while in this study the GERG-2008 is adopted, based on the validation results.

6. Sensitivity analysis results and discussion

In this section the results of the performed sensitivity analyses are reported. Three different parameters are evaluated in the sensitivities:

- The heat provided by the ASU, in order to assess the effect of the heat integration between ASU and the Allam cycle.
- The purity of the oxygen provided by the ASU.
- The size of the power plant.

6.1. Sensitivity on size

The objective of this sensitivity analysis is to assess the performance of the Allam cycle as the power output varies by considering the following sizes (net electric power):

- 400 MW, corresponding to the maximum single train size of a cryogenic ASU.
- 300 MW.
- 200 MW.
- 100 MW.
- 50 MW

For all these sizes, the ASU oxygen purity of 99.5 % and the plant modelling assumptions detailed Section 3 are considered for all the cycle components. Such assumptions allow to account for the influence of plant size (volumetric flow rate) on the design and efficiency of the compressors, turbine, electric drivers and generators. Owing to the lack of literature data, no size effect is considered on the specific power consumption of the ASU, resulting in a possible overestimation of the performance for the small size plants.

The efficiency of each gas phase and dense phase compressor has been assessed using the methodology and assumptions described in Section 3.2, evaluating the need of using gearboxes by means of a preliminary estimate of the compressor rotational speed using the Balje diagram. The results of the performance assessment for all the considered plant sizes are reported in Appendix. The tables detail the values of isentropic efficiency, mechanical efficiency (including shaft bearing and gearbox, if required) and electrical efficiency. A preliminary mechanical efficiency value of 99.90 % has been considered for the shaft bearings.

The results show how for plant sizes of 200 MW and larger, all the gas phase compressors have synchronous rotational speed (no need of gearbox). Only for the 100 MW and 50 MW plants the limited inlet volumetric flow rate makes it necessary to adopt a gearbox for the compressors. However, the same rotational speed (i.e., 6000 rpm for the 100 MW plant, 8000 rpm for the 50 MW plant) is suitable for all the gas phase compressors as well as the first dense phase compressor (pump 1).

The dense phase compressors require a higher rotational speed (i.e., a gearbox) in all analyzed plant sizes. In particular, pump 2 and oxy pump feature similar optimal rotational speeds, thus an installation on the same shaft could be an option, adopting a single electric driver and gearbox. On the other hand, it must be noted that this solution may

Table 10
Summary of cost models used to assess the bare module cost of the cycle equipment units.

List of Components	Size Parameters	Reference Size	Reference Cost [M$ 2015]	Scale Factor	Reference
ASU	O2 flow, kgO2/s	61.00	120.365	0.60	Derived from [1]
CPU	CO2 flow, kgCO2/s	88.80	35.200	0.60	Derived from [1]
Turbine	Gross power, MW	300.00	32.550	0.60	Average gas and steam turbine
Recuperator SS	Area, m2	10000.00	2.500	0.91	Derived from [1]
Recuperator Inconel	Area, m2	10000.00	12.500	0.91	5 times stainless steel
HXs and Coolers	Area, m2	500.00	0.400	0.60	[40]
Recycle, O2 and Fuel Compressors	Power, MW	27.40	21.500	0.67	[39]
BOP of total plant (civil works + control instrumentation, etc.)	Fuel input, MW	1536.00	125.818	0.30	Derived from [1]

Table 11
Main results of the Allam cycle 400 MW base case.

	Unit	
Recycle Mass Flow Rate, stream 5	kg/s	515
Regenerator moderator and oxidant outlet temperatures, streams 4 and 5	°C	697.9
Combustor outlet temperature, stream 6	°C	1167.7
Turbine inlet mass flow rate, stream 6	kg/s	1109.6
Turbine cooling flow mass flow rate, stream 7	kg/s	150.4
Turbine cooling temperature, stream 7	°C	437.9
Turbine outlet temperature, stream 8	°C	724.9
Turbine outlet pressure, stream 8	bar	30.6
Regenerator flue gases outlet temperature, stream 9	°C	56
Dense phase compression pressure, stream 12	bar	80
Captured CO_2 mass flow rate, flow 22	kg/s	42.2
ASU input air mass flow rate, flow AIR	kg/s	262.6
Oxygen mass flow rate, flow 17	kg/s	58.4
Power Block		
Thermal Power of fuel input	MWth	730.45
Turbine Gross Electric Power	MWel	588.03
Recycle Compression Power	MWel	87.54
Oxidant Compression Power	MWel	17.25
NG Compression Power	MWel	7.71
ASU Power	MWel	80.84
CPU Power	MWel	6.31
Net Power Out	MWel	388.38
Overall net electric efficiency	%	53.17 %
CO2 Capture Level	%	99.05
Specific CO2 Emissions	gCO2/kWh	3.45

penalize the operability of the plant.

As far as efficiency is concerned, the biggest penalty appears to be the adoption of the gearbox for the gas phase compressors, affecting the plants with sizes below 200 MW.

The results of the cycle simulations at different plant sizes are reported in Table 12. It is important to notice that, when varying the plant size, the variation of turbine performance (isentropic efficiency and cooling flow requirement) generates a variation in the ratio between TIT and TOT. Thus, to keep the TOT to the maximum value (this way maximizing the preheating in the regenerator, with a positive effect on the efficiency) with a fixed turbine inlet pressure, it is necessary to vary either the TIT or the turbine outlet pressure. Varying the TIT would causes a variation of the recycle flow rate, ultimately resulting in compromising the heat balance of the recuperator. Hence, for all the considered cases optimizing the turbine outlet pressure to have TOT = 725 °C and recuperator approach point at 20 °C results in a higher efficiency than varying the TIT.

The results reported in Table 12 highlight the following issues:

The 300 MW plant requires appreciably more cooling flows (+5.4 %) than the 400 MW plant due to the suboptimal rotational speed of the turbine (as explained in Section 3.4). As a consequence, to achieve the target TOT of 725 °C, it is necessary to either increase the TIT or the turbine outlet pressure. According to our simulation results, the second option turns out to be more efficient (+0.39p.p. of overall plant efficiency).

The 200 MW plant needs appreciably less cooling flow (due to the more loaded stages) than the 400 MW and 300 MW cases. As a result, it requires a lower turbine outlet pressure. Simulation results indicate that the best option in terms of overall plant efficiency is a TOP of 24 bar with a gain in the net plant efficiency of 0.21p.p. This result can be explained looking at the composite curve (T-Q diagram, reported for BC in Fig. 11) of the recuperator: if the moderator flow rate increases, the recuperator lacks high temperature heat to preheat the larger moderator flow, with the net effect of increasing the hot side approach temperature difference to 40 °C (with large heat transfer exergy losses). For this reason, even though reducing the TOP to 24 bar increases the power required by the CPU compressors, the effect on the overall plant efficiency is positive. Thanks to the reduced amount of turbine cooling flows, the overall net electric efficiency of the plant (53.38 %, delivering CO_2 at 110 bar) is higher than the one of the larger size 300 MW plant (52.46 %, delivering CO_2 at 110 bar). Interestingly, the advantage of having a proper turbine design more than offsets the penalty caused by the mechanical losses of the turbine gearbox.

The 100 MW plant resembles the 200 MW one, due to the optimized rotational speed of the turbine. The lower isentropic, mechanical and electrical efficiencies of the compressors cause an efficiency penalty of 1.55p.p. compared to the 200 MW case. Such penalty is mainly due to the need of adopting a gearbox for the gas phase compressors. The efficiency of uncooled 50 MW case is highly penalized by the unbalance of the heat capacities of the streams in the recuperator, leading to a large delta T approach at its hot end (about 80 °C vs the 20 °C approach adopted in the cases with cooled turbine). Moreover, the lower TIT (950 °C) reflects on a lower TOT, thus reducing the preheating of the recycled flows, with an additional detrimental effect on the efficiency.

As it can be seen from the results plotted in Fig. 8, adjusting the turbine outlet pressure depending on the plant output has a positive effect on efficiency: for the whole range of power output, it is found to have a higher or equal efficiency than increasing the TIT. It is important to recall that the analysis performed in this study does not consider the size effects on the specific energy consumption of the ASU. Thus, the figures of net plant electric efficiency should be reviewed in light of more accurate estimates of the ASU power consumption at the different plant sizes.

Table 12 compares the efficiency figures calculated for the different plant sizes. Some conclusions can be drawn from the reported results:

- In all the cases the optimal working point (i.e., the one maximizing efficiency) is found for the minimum temperature difference on the hot side of the regenerator (20 °C), with the only exception of the 50

Table 12
Summary of the key simulation results for the sensitivity on the plant size.

	Unit	BC	PS-300	PS-200	PS-100	PS-50
Recycle Mass Flow Rate, stream 5	kg/s	515	414	200	100	114.97
Regenerator moderator and oxidant outlet temperatures, streams 4 and 5	°C	697.9	704.8	698	697.5	586.9
Combustor outlet temperature, stream 6	°C	1167.7	1159.6	1219.0	1218.6	950
Turbine inlet mass flow rate, stream 6	kg/s	1109.6	859.9	497.6	248.8	198.5
Turbine cooling flow mass flow rate, stream 7	kg/s	150.4	136.6	68.8	38.4	–
Turbine cooling temperature, stream 7	°C	437.9	417.6	454.9	472.0	–
Turbine outlet temperature, stream 8	°C	724.9	724.8	725.0	724.5	631.9
Turbine outlet pressure, stream 8	bar	30.6	34	24.0	24.0	35
Regenerator flue gases outlet temperature, stream 9	°C	56	54.3	60.5	60.2	53.1
Dense phase compression pressure, stream 12	bar	80	80	80	80	80
Captured CO_2 mass flow rate, flow 22	kg/s	42.2	31.6	21.1	10.5	5.9
ASU input air mass flow rate, flow AIR	kg/s	262.6	196.9	131.3	65.6	36.9
Oxygen mass flow rate, flow 17	kg/s	58.4	43.8	29.2	14.6	8.19
Thermal Power In	MWth	730.45	547.84	365.23	182.61	102.30
Turbine Gross Power	MWel	588.03	435.91	297.79	148.359	78.6878
Recycle Compression Power	MWel	87.54	64.52	46.23	25.37	13.08
Oxidant Compression Power	MWel	17.25	13.04	8.79	4.46	2.53
NG Compression Power	MWel	7.71	5.66	3.85	1.93	1.08
ASU Power	MWel	80.84	60.63	40.43	20.21	11.33
CPU Power	MWel	6.31	4.53	3.53	1.75	0.83
Net Power Out	MWel	388.38	287.41	194.95	94.64	49.85
Overall Efficiency	%	53.17	52.46	53.38	51.83	48.73
CO2 Capture Level	%	99.05	99.05	99.06	99.06	99.02
Specific CO2 Emissions	gCO2/kWh	3.45	3.51	3.54	3.59	4.02

MW case, where the cycle conditions made impossible reaching an approach temperature difference lower that 80 °C. In this case the low TIT (due to the uncooled turbine) requires a proportionally larger recirculated flow and the available heat is not enough to achieve such a small temperature approach.

- The reduction of the plant size reflects in an efficiency reduction, with the exception of the 200 MW case: as explained before, this is related to the sub-optimal rotational speed of the turbine in the 300 MW case (still slightly suboptimal also for the 400 MW case) caused by the absence of gearboxes for such turbine sizes.
- The CO_2 capture level and specific emissions remain almost constant with size.

6.2. Sensitivity on oxygen purity

In this section the effects of oxygen purity on the performance of the Allam cycle are evaluated. The analysis is performed considering a large size Allam cycle with net power output of about 400 MW cycle. According to our information (e.g., the IEA GHG study [8]), such size should correspond to the maximum available size of ASU trains. The range 95 %-99.5 % oxygen purity range (molar basis) is considered because it corresponds to the typical purity range for cryogenic ASUs. The electric power consumption of the ASUs for the different levels of purity has been taken from the curves reported in ref. [41]. An important issue arising when using low-purity oxygen is the progressive increase in incondensable gases (N2, O2 and Ar) in the recycled stream. This causes the following problems:

1) The presence of O_2 and N_2 leads to the increase of the critical temperature of the mixture causing the risk of having a two-phase flow at the inlet of the dense phase compressors (steams 12 and 18 as in Fig. 1). This issue is addressed by increasing the pressures of these flows, as will be detailed in the following.
2) The compression power increases because of two reasons: (i) the larger volumetric flow rate of recycled flow due to incondensable gases, (ii) the higher pressure that has to be reached in the gas phase compression (occurring with larger specific volume, thus more energy intensive).

On the other hand, N_2 and O_2 feature a specific heat capacity increasing with temperature, an opposite behavior than supercritical CO_2. Thus, their presence in the recycled streams might help reducing the specific heat capacity of the recycled streams in the medium–low temperature range, with a beneficial effect on the heat balance of the recuperator.

Table 13 reports the compositions (molar basis) of the streams 12 and 18 (referred to Fig. 1) for the three different oxygen purity cases. In order to assess if these streams are in two phase conditions at the plant operating conditions, the phase diagrams of CO_2-N_2, CO_2-Ar and CO_2-O_2 mixtures at relevant temperatures and pressures obtained from experimental data and presented in [37,78] were used. Since the phase diagrams are only provided for binary mixtures, for each stream and each oxygen purity the conditions were evaluated assuming that all the impurities were constituted by the main impurity of the stream (N_2 for stream 12 and O_2 for stream 18). Given the conditions reported in Table 13, from the analysis resulted that:

- For all the cases stream 18 is outside the two-phase region at the plant operating conditions, therefore the oxidant compression is reasonably safe.
- For the 99.5 % ASU purity case, a pressure of 80 bar is sufficient to keep the condition of stream 12 outside the two-phase region of the diagram also for temperatures down to 20 °C. However, according to the vapor liquid equilibrium curves of ref. [37,78] obtained for CO_2-N_2 mixtures at a temperature of 20 °C, for the cases with oxygen purity below 97.5 % (97 % and 95 %), the pressure of the stream must be increased to 120 bar in order to have a sufficient safety margin from the saturated liquid line (thus, to avoid liquid formation at compressor inlet). For the intermediate oxygen purity cases (i.e., 98 % and 98.5 % oxygen purity), a pressure of 100 bar is sufficient.

It is important to notice that increasing the pressure of stream 12 from 80 bar to 100 bar or 120 bar causes two important negative effects on the cycle efficiency:

1. it increases the pressure ratio of the gas-phase compressors (featuring a larger specific power consumption owing to the lower gas density) and decreases the pressure ratio of the dense-phase compressors.
2. It makes it necessary to remove the fourth intercooled gas compressor stage (CPR-4 and related intercooler) because its inlet stream would be at about 80–90 bar with the risk of having a liquid

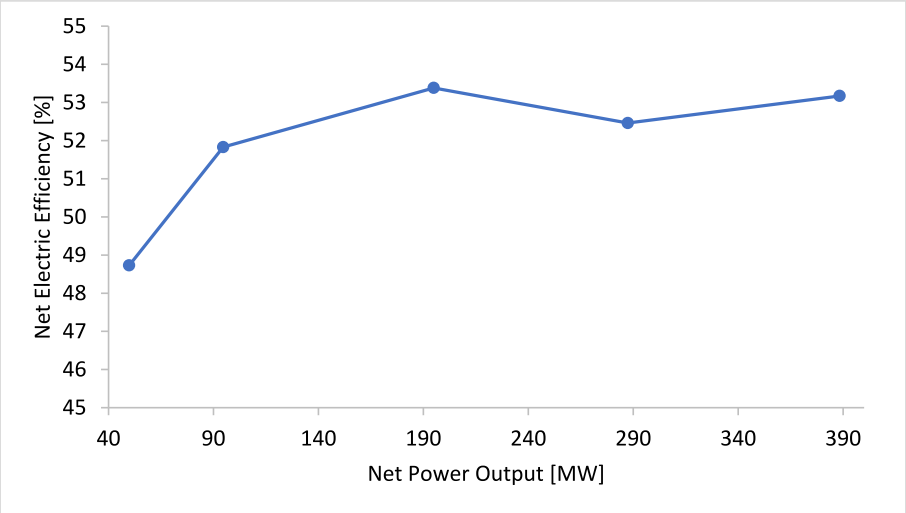

Fig. 8. Net Electric Efficiency of the Allam cycle as a function of the net power output.

Table 13
T, p and molar-based composition of the streams 12 and 18 in the three cases considered. Streams are referred to the numbering in Fig. 1.

Component	Stream # 12			Stream # 18		
	BC	OP-97	OP-95	BC	OP-97	OP-95
CO2	97.995 %	93.426 %	89.911 %	84.957 %	80.675 %	77.384 %
H2O	0.137 %	0.136 %	0.136 %	0.119 %	0.118 %	0.117 %
O2	0.117 %	0.118 %	0.120 %	13.340 %	13.340 %	13.340 %
N2	1.183 %	2.618 %	2.594 %	1.524 %	2.397 %	3.312 %
AR	0.568 %	3.702 %	6.239 %	0.532 %	3.697 %	5.848 %
T [°C]	26.0	26.0	26.0	17.4	16.6	16.0
P[bar]	80	120	120	120	120	120

phase. Thus, the cycle designs with 95 %-98.5 % oxygen purity feature only three intercooled stages of the gas phase compression.

The resulsts of the simulations and cycle efficiency optimization made for the different levels of oxygen purity are reported in Fig. 9 and Table 14. Fig. 9 indicates that, in the range 95 %-98.5 % oxygen purity, the power block (Allam cycle without ASU and CPU) and net plant efficiency (includingthe auxiliary power consumption of the ASU) increases slightly with the oxygen purity. In particular, the net plant efficiency rises from 51.7 % at 95 % purity to 52.0 % at 98.5 %. However, there is a more appreciable efficiency improvement when passing from 98.5 % to 99 % purity, which features a net electric plant efficiency of 53.3 %.

The performance results reported in Table 14 indicate that, for the same pressure ratio and inlet stream conditions, the cases with lower oxygen purity feature a larger turbine power output but also a higher recycle compression power consumption. This is due to the increase in specific volume caused by the presence of incondensable gases. For instance, the case with 95 % purity features a turbine power output which is approximately 15 MW larger than the 99.5 % purity case. However, the presence of incondensable gases causes also a significant increase in compression power (approx. + 29 MW in case of 95 % purity oxygen) which outweighs the beneficial effect on the turbine.

The compression power appears to be also the reason behind the more appreciable efficiency increase when passing from 98.5 % oxygen purity to 99.0 %. The causes are:

- The build-up of incondensable gases in the recycle stream which have a negative effect decreasing the supercritical fluid density (from 800.6 kg/m^3 to 788.7 kg/m^3). The build-up is emphasized by the large recycle ratio (i.e., the ratio between the recycled working fluid and the fraction sent to capture, equal to 27.9). For example, the case with 99 % oxygen purity has a CO_2 concentration of 97.1 % while the case with 98.5 % has a concentration of 96.2 %.
- The need of increasing the pressure of the gas-phase compressors from 80 bar to 100 bar so as to avoid the formation of a liquid phase at the inlet of the dense phase compressors.

Fig. 9 indicates also that the effect of the oxygen purity is larger on the efficiency of the power block (Allam cycle without ASU and CPU). This occurs because the specific power consumption of the ASU increases with the oxygen purity, reducing the benefit of adopting high purity oxygen.

As for the effect of the number of intercoolers of the gas phase compression train, the plot of Fig. 9 indicates that the effect on cycle efficiency is minor: if the 99 % and 99.5 % oxygen purity cases are designed with only three intercooled stages, their efficiency is still considerably higher than the cases with lower purity.

Finally, it is important to notice that the efficiency optimal oxygen-purity might not coincide with the economically optimal solution (i.e., the solution minimizing the Cost of Electricity) because the designs with 97 % and 95 % O_2 purity feature:

- Simpler and less expensive ASU configurations.
- Probably less expensive compression trains, lacking the dense phase compressor between 80 and 120 bar and the fourth stage of the intercooled gas compressor.

However, to perform an economic analysis on this topic consistent and accurate capital cost data for the three different types of ASUs, currently unavailable in literature, would be necessary. Future studies, hopefully in collaboration with ASU manufacturers or providers, could investigate such economic comparison.

6.3. *Sensitivity on the thermal power recovered from the ASU*

Another fundamental aspect to be considered in the assessment of the plant efficiency is the amount of heat provided by the ASU main air compressor to the regenerator. In order to assess the effects of such an important factor, a sensitivity analysis is performed, considering a variation range from zero to twice the value considered in the base case. For all cases, the ASU with 99.5 % oxygen purity is considered.

The results of the analysis are reported in Table 15, where the name

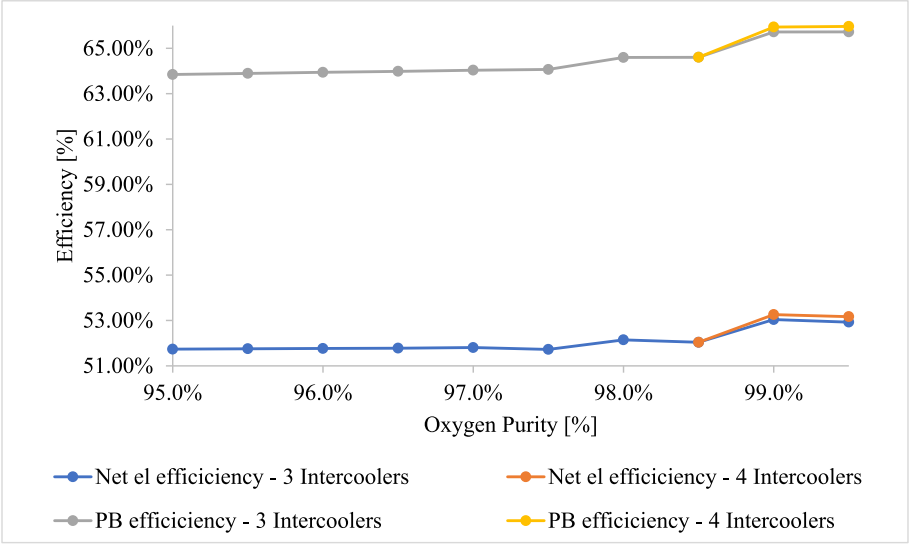

Fig. 9. Net Electric Efficiency of the Allam cycle as a function of oxygen purity. The grey and yellow lines denote the efficiency of the power block (PB) without considering the power consumption of the ASU and CPU. The blue and orange lines indicate the efficiency of the total plant (including ASU and CPU power consumption). (For interpretation of the references to colour in this figure legend, the reader is referred to the web version of this article.)

Table 14
Results of the cycle simulations for different levels of O2 purity provided by the ASU.

	Unit	OP-95	OP-97	BC
Recycle Mass Flow Rate, stream 5	kg/s	490	510	515
Regenerator moderator and oxidant outlet temperatures, streams 4 and 5	°C	704.3	703.5	697.9
Combustor outlet temperature, stream 6	°C	1202.3	1184.8	1167.7
Turbine inlet mass flow rate, stream 6	kg/s	1076.8	1100	1109.6
Turbine cooling flow mass flow rate, stream 7	kg/s	212.7	173.4	150.4
Turbine cooling temperature, stream 7	°C	523.4	467.3	437.9
Turbine outlet temperature, stream 8	°C	724.3	724.5	724.9
Turbine outlet pressure, stream 8	bar	30.6	30.6	30.6
Regenerator flue gases outlet temperature, stream 9	°C	68.3	62.2	56
Dense phase compression pressure, stream 12	bar	120	120	80
Captured CO_2 mass flow rate, flow 22	kg/s	45.3	43.9	42.2
ASU input air mass flow rate, flow AIR	kg/s	262.6	262.6	262.6
Oxygen mass flow rate, flow 17	kg/s	61.6	60.1	58.4
Power Block				
Thermal Power In	MWth	730.45	730.45	730.45
Turbine Gross Power	MWel	603.62	597.44	588.03
Recycle Compression Power	MWel	116.05	109.80	87.54
Oxidant Compression Power	MWel	19.40	18.42	17.25
NG Compression Power	MWel	7.71	7.71	7.71
ASU Power	MWel	76.17	76.88	80.84
CPU Power	MWel	6.14	6.21	6.31
Net Power Out	MWel	377.91	378.43	388.38
Net Electric Plant Efficiency	%	51.74 %	51.81 %	53.17 %
CO_2 Capture Level	%	94.84	96.76	99.05
Specific CO_2 Emissions	gCO_2/kWh	20.32	12.65	3.45

AHI-NO indicates the case without heat integration with the ASU, the base case (BC) is the 99.5 % oxygen purity case as indicated in the previous section, and the case AHI-AD considers that the heat provided by the ASU (and/or external processes) is twice the value assumed in the base case. In case AHI-AD, the additional external heat is used to decrease the hot side temperature differences of the regenerator from 20 °C to 10 °C (i.e., preheating more the moderator and oxidant). As can be seen from the results in Table 15, the amount of heat provided by the ASU has a strong impact on the plant's performance. Compared to the base case, the case AHI-AD has a net electric efficiency which is 2.93 percentage points higher (56.10 % vs. 53.17 %). Such an improvement in efficiency is especially remarkable if we consider that it is just due to the integration of the cycle with medium–low temperature waste heat. Similarly, in the opposite situation, if the Allam cycle cannot recover any external heat (case AHI-NO), the net electric efficiency drops to 50.11 % (-3.06p.p.). Indeed, without heat integration with external sources, it is impossible to keep the temperature difference on the hot side of the regenerator to the design 20 °C and its value increases to 44 °C.

Fig. 10, Fig. 11 and Fig. 12 show the T-Q diagram (also called "composite curve", where the hot and cold streams contributions are grouped depending on the temperature range of each stream) of the regenerator in the three different cases. Fig. 10 indicates that, in absence of heat integration with external sources, the pinch point at about 110 °C, combined with the larger heat capacity flow rate (slope of the composite curve, dQ/dT) of the cold streams, does not allow pre-heating the moderator and oxidant to a temperature close to the inlet one of the flue gases. Figs. 11 and 12 show that the addition of external waste heat (coming from the ASU or other sources) increases the heat capacity flow rate of the hot composite curve making it possible to heat the cold streams to a temperature much closer to that of the inlet flue gases. Indeed, in the BC case the hot and cold composite curves are nearly parallel, and the temperature difference on the hot side of the regenerator can be reduced to 20 °C. In the AHI-AD case the large availability of medium temperature heat allows preheating the moderator and oxidant flows to 715 °C, only 10 °C lower than the TIT.

In conclusion, the net efficiency of the Allam cycle is strongly dependent on the hot side temperature difference of the regenerator: the lower the temperature difference, the higher the cycle efficiency. This is not surprising because reducing the hot side temperature difference means reducing the fuel consumption of the combustor to achieve the target (optimal) TIT. It is worth noticing that, when passing from case AHI-NO to BC, the medium–low temperature external heat provided to the Allam cycle (about 54 MW) is converted into electricity with a marginal efficiency of 41 %, a very high value for waste heat recovery. Similarly, when passing from case BC to AHI-AD, the additional external heat (another 54 MW) is converted into electricity with a marginal efficiency of 35 %, still representing a good conversion efficiency for waste heat. Fig. 13 shows the net electric efficiency of the plant as a function of the heat recovered from the ASU.

Table 15
Results of the sensitivity on the heat from ASU.

	Unit	AHI-NO	BC	AHI-AD
Recycle Mass Flow Rate, stream 5	kg/s	470	515	580
Regenerator moderator and oxidant outlet temperatures, streams 4 and 5	°C	672.4	697.9	707.7
Combustor outlet temperature, stream 6	°C	1163.4	1167.7	1151.9
Turbine inlet mass flow rate, stream 6	kg/s	1064.8	1109.6	1174.3
Turbine cooling flow mass flow rate, stream 7	kg/s	130.2	150.4	157.1
Turbine cooling temperature, stream 7	°C	400.8	437.9	471.6
Turbine outlet temperature, stream 8	°C	723.4	724.9	717.7
Turbine outlet pressure, stream 8	bar	30.6	30.6	30.6
Regenerator flue gases outlet temperature, stream 9	°C	48.6	56	60.6
Dense phase compression pressure, stream 12	bar	80	80	80
Captured CO_2 mass flow rate, flow 22	kg/s	42.2	42.2	42.2
ASU input air mass flow rate, flow AIR	kg/s	262.6	262.6	262.6
Oxygen mass flow rate, flow 17	kg/s	58.4	58.4	58.4
Power Block				
Thermal Power In	MWth	730.45	730.45	730.45
Turbine Gross Power	MWel	560.13	588.03	615.53
Recycle Compression Power	MWel	81.96	87.54	93.66
Oxidant Compression Power	MWel	17.26	17.25	17.24
NG Compression Power	MWel	7.71	7.71	7.71
ASU Power	MWel	80.85	80.84	80.84
CPU Power	MWel	6.31	6.31	6.31
Net Power Out	MWel	366.05	388.38	409.77
Overall Efficiency	%	50.11 %	53.17 %	56.10 %
CO_2 Capture Level	%	99.05	99.05	99.05
Specific CO_2 Emissions	gCO_2/kWh	3.67	3.45	3.28

7. Economic analysis results and discussion

This section reports the results of the economic analysis of the 400 MW base case Allam cycle power plant under the assumptions listed in Section 4. Table 16 details the breakdown of the equipment total capital requirement. Fig. 14 shows that the ASU has the major equipment cost, with the turbine, regenerator and recycle compressors representing the other most significant components. The total capital requirement of the cycle turns out to be 2.490 €/kW, reflecting on a COE of 127.8 €/MWh. This value is significantly higher than the 83.6 €/MWh found in [2] with the same costing procedure. The difference between the two costs lies in the assumptions:

- First of all, the present study considers a natural gas cost of 12 €/GJ, while 8 €/GJ was assumed in [2]. If such an assumption looked reasonable in 2015, the strong fluctuations of the gas price (especially in the European market) in the past years require a higher base case cost to be considered. For natural gas cost of 8 €/GJ. As can be seen from the sensitivity on the natural gas cost reported in Fig. 16, this difference increases the COE of more than 20 €/GJ, being fuel the most important influence factor on the COE (see Fig. 15 for details).
- All the cost values are actualized to 2022 by means of the CEPCI index. Given the strong inflation of the last few years, the ratio $CEPCI_{2022}/CPECI_{2014}$ is 1.41, reflecting on a significant increase in the investment cost. Moreover, the €/$ change is assumed to be equal to the average change in the period 2014–2022, introducing an additional difference in the cost calculations.
- The value of efficiency assessed in [2] is almost 2 % higher than the one of the present studies, due to some differences in the cycle modelling. The main differences are the thermal oil loop delivering the ASU heat to the regenerator (reducing the available temperature of such heat, thus the efficiency of the cycle) and the turbomachinery efficiency: the values found with the more accurate assumptions of this study are slightly lower than the ones assumed in [2].

Table 17 and Fig. 15 report the main results of the economic analysis comparing the Allam cycle with the benchmark NGCC with post-combustion capture. Despite its smaller size (400 MW vs. 650 MW of net power), the Allam cycle features a lower specific capital cost (−20 %) and a similar efficiency to the reference NGCC with post-combustion capture. Therefore, when looking at the cost of electricity, it has very similar capital and fuel cost components. Compared to the NGCC, the Allam cycle is expected to benefit from the lower O&M costs and, especially, lower CO_2 emission taxes thanks to the higher CO_2 capture level. This results in a COE which is 13.3 €/MWh lower with respect to the benchmark cycle. It is also worth noting that the most important cost component is, for both the cycles, the fuel cost, thus reflecting on the importance of research and development towards higher efficiency solutions.

Moreover, a sensitivity analysis on the natural gas cost has been performed evaluating the COE of the two compared power plants. The results, that can be seen in Fig. 16, show that the Allam cycle, thanks to the lower emissions and capital cost, has a lower COE than the NGCC

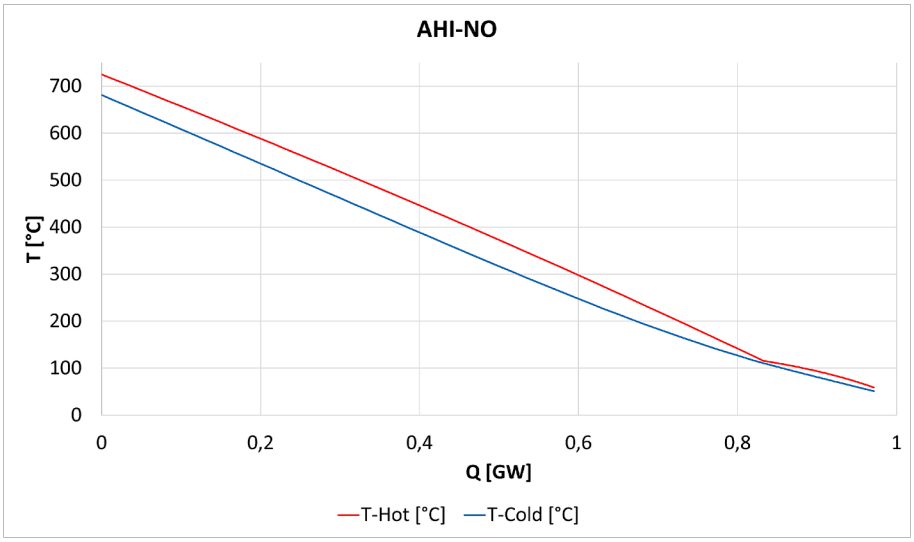

Fig. 10. T-Q diagram of the AHI-NO case (without heat integration with external sources).

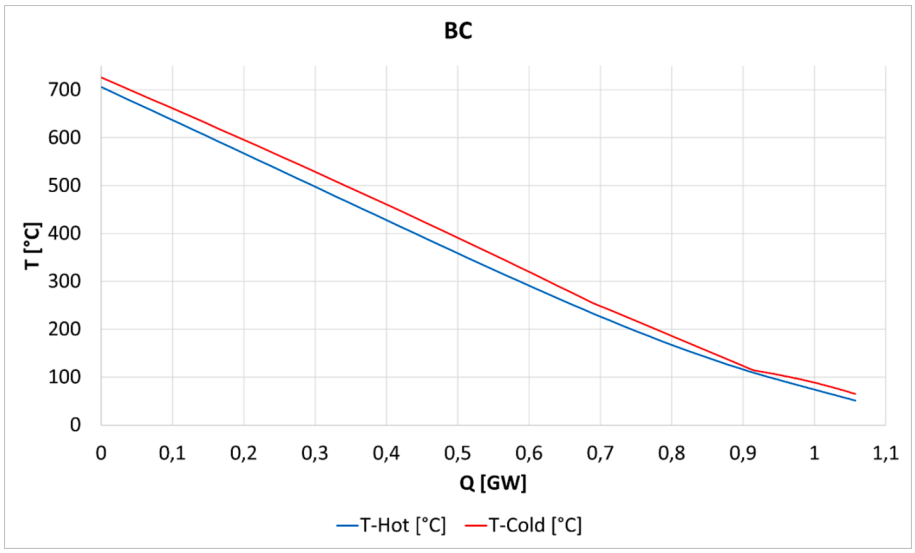

Fig. 11. T-Q diagram of the BC case (where the regenerator recovers heat from the main air compressor of the ASU).

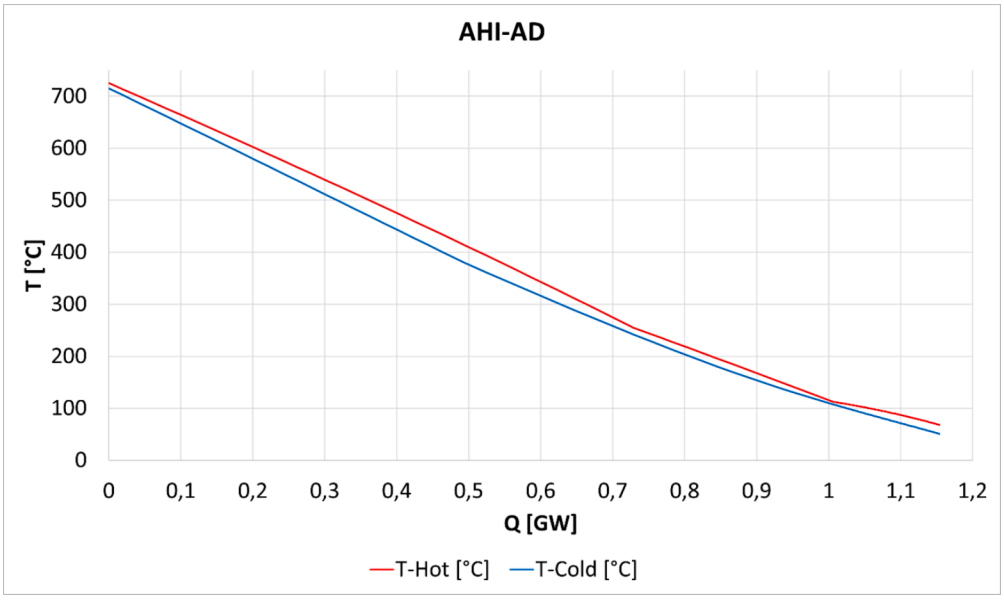

Fig. 12. T-Q diagram of the AHI-AD case.

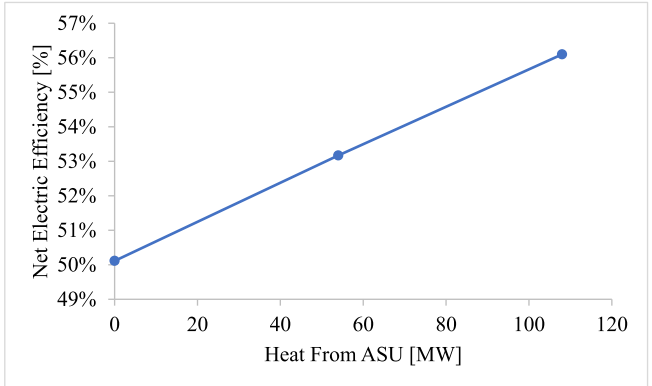

Fig. 13. Net Electric Efficiency of the large scale Allam cycle (Cases AHI–NO, BC and AHI-AD) as a function of the heat provided by the ASU and/or external processes.

Table 16
Allam cycle equipment total capital requirement breakdown in M€.

Unit	Total Equipment cost [M€]	Total installed cost [M€]	Total capital Requirement [M€]
ASU	125.01	250.02	315.45
Turbine	56.92	113.83	143.62
Regenerator	37.11	74.22	93.65
Recycle Compressors	48.45	96.89	122.25
CPU	29.50	59.00	74.44
All Others	6.55	13.09	16.52
BOP	79.35	158.69	200.22
Total	382.88	765.76	966.16

with Cansolv regardless of the NG cost. Given its slightly higher efficiency, it also features a lower COE increase as a function of the NG cost increase. In fact, the slope of the lines is inversely proportional to the efficiency of the cycles: the higher is the cycle efficiency, the less steep is

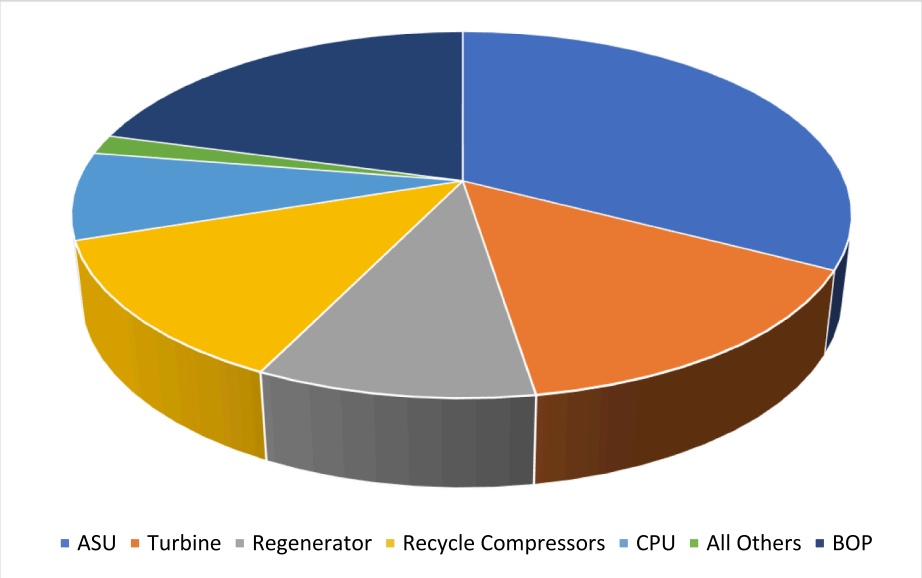

Fig. 14. Shares of the different components in the overall capital cost.

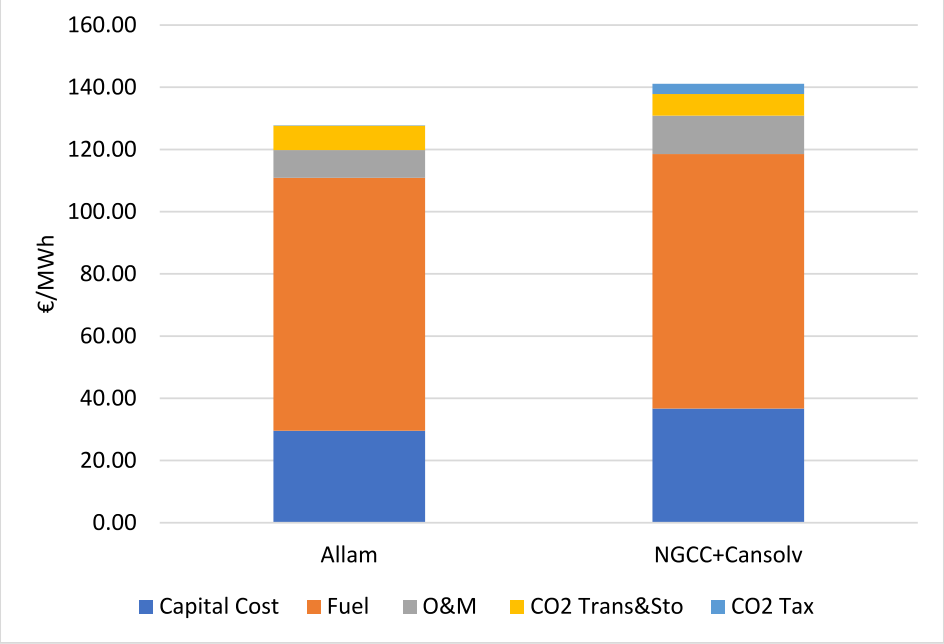

Fig. 15. Components of the Cost of electricity (COE) for the two analyzed plants.

the line. On the other hand, since the efficiency is similar (53.1 % vs 52.8 %), the difference in slope is negligible.

Fig. 16 also shows the effect of a higher (doubled) cost of the expander on the COE of the Allam cycle (BC-HTC): given its low technology readiness level, this cost item is very uncertain. Nevertheless, the results of the sensitivity indicate that such an increase would not impact the overall COE significantly, and the Allam cycle would remain economically competitive also for an expander cost 100 % higher than the value assumed in this study.

8. Conclusions

This work has investigated the energy and economic performance of the Allam cycle in its basic configuration (without recompression), evaluating how the cycle size, oxygen purity and waste heat integration affect such performance. The analysis is based on a process model of the overall cycle including the CO_2 purification unit and preliminary 1-D design models of the turbine and recuperative heat exchangers.

The base case utility scale plant (388 MW of net power output) thermally integrated with the air separation unit is expected to achieve a net electric efficiency of approximately 53.17 %, a lower value than those found in previous works (in the range 54–55 % for similar cycle assumptions). The difference in efficiency is due to the inclusion of power consumption of the CO_2 purification unit, the temperature drop caused by the hot oil loop between the ASU and the power block, and more conservative assumptions for the electrical and mechanical efficiencies of the turbomachines.

Cycle simulations indicate that the optimal oxygen purity for the efficiency of the overall plant (cycle and air separation unit) is 99.5 % (molar basis): in fact, the higher energy consumption of the ASU to

Table 17
Economic analysis results of the 400 MW Allam cycle and of the F-class 650 MW NGCC with post combustion CO2 capture system (based on CANSOLV) assessed in ref. [3]. Fuel costs, CO2 transport costs and CO2 emission tax have been updated with the assumptions adopted in this study.

	Allam	NGCC + Cansolv [3]
Thermal Power In [MW]	730.5	1222.9
Cycle Power [MW]	388.1	646.0
Net electric efficiency [%]	53.17 %	52.80 %
Cycle Bare Investment Cost [M€]	382.9	986.5
Installation factor and contingencies	2	1.512
Total plant cost [M€]	765.8	1502.4
Specific inv cost [M€/MW]	1.973	2.326
Specific Total Capital Requirement [M€/MW]	2.490	3.089
Total Capital Requirement [M€]	966.2	1995.3
OPERATING COSTS		
Natural Gas cost [M€/y]	248.8	416.5
Chemicals cost [M€/y]	0.8	9.3
MAINTENANCE COSTS		
New technologies [M€/y]	5.4	0.0
Conventional technologies [M€/y]	10.0	14.6
OTHER COSTS		
Insurance Costs and Taxes [M€/y]	4.4	19.2
Labor costs [M€/y]	3.7	9.4
Administrative costs and overhead [M€/y]	2.9	2.4
Carbon Tax [M€/y]	0.5	16.7
CO_2 Transport & storage cost [M€/y]	23.9	35.4
COE [€/MWh]	127.8	141.1

produce purer oxygen is outweighed by the lower work required in the compression phase. Cases with lower oxygen purity are penalized by the build-up of inert gases (N_2 and Ar) which increase the compression power.

The sensitivity analysis on the heat integration with external sources shows that the stand-alone case (not thermally integrated with the ASU or other external processes) can achieve a net electric efficiency of about 50 % which is 3 percentage points lower than the base case (approximately 53 %). If the thermal power recovered from external sources (e.g. ASU) is doubled compared to the base case, the net electric efficiency increases to about 56 %. Thus, the Allam cycle can convert low-medium temperature waste heat recovered from the ASU (or external processes) with a very good marginal efficiency, ranging from 35 % (when available external heat accounts for about 10 % of the total regenerator heat) to 41 % (when available external heat accounts for about 5 % of the regenerator heat). Given the importance of the additional low temperature heat at the regenerator, adopting a recompression cycle arrangement, as proposed in [16,21], may be beneficial. This will be investigated in future works.

As far as the plant size is concerned, the cycle efficiency remains relatively high (> 51 %) in the range 400 MW-100 MW. Compared to utility size plants, smaller size plants can benefit from the availability of gearboxes for the turbine. This allows to target a more compact turbine design, requiring a lower number of stages (5 instead of 6–8 of utility scale plants) and cooled stages (4 stages instead of 5). Reducing the number of stages generates a saving in terms of turbine coolant, with beneficial effects on the cycle performance. The analysis has also investigated a 50 MW plant, featuring an uncooled turbine with a TIT limited to 950 °C. The calculated net electric efficiency of such cycle is found to be 48.7 %, appreciably lower than the other plant sizes. The main reason appears to be the limited TOT, which has a detrimental effect the heat integration in the recuperator, reflecting on a higher temperature difference on the hot side of the exchanger and a lower preheating temperature of the recirculated flows.

Moreover, the economic analysis has highlighted that, despite its smaller plant size, the specific total capital requirement of the utility scale (400 MWel) Allam cycle is 2490 €/kWel, 20 % lower than the reference 650 MWel combined cycle with Cansolv system for post-combustion capture. When looking at the cost of electricity, the two cycles feature very similar capital and fuel cost components (i.e., the fuel cost is similar because the two plants have similar efficiency). Compared to the NGCC, the Allam cycle is expected to benefit from the lower O&M costs and, especially, lower CO_2 emission taxes thanks to the higher CO_2 capture level. This benefits result, according to our estimates, in a COE which is approximately 13.3 €/MWh lower (−10 %) with respect to the benchmark NGCC cycle.

Future works will focus on the evaluation of Allam cycle scheme with recompression, as proposed in refs. [11,16].

CRediT authorship contribution statement

Matteo Martinelli: Writing – original draft, Visualization, Validation, Software, Methodology, Data curation, Conceptualization. **Paolo Chiesa:** Writing – review & editing, Validation, Supervision, Methodology, Investigation, Conceptualization. **Emanuele Martelli:** Writing – review & editing, Validation, Supervision, Software, Resources, Project administration, Methodology, Investigation, Funding acquisition, Conceptualization.

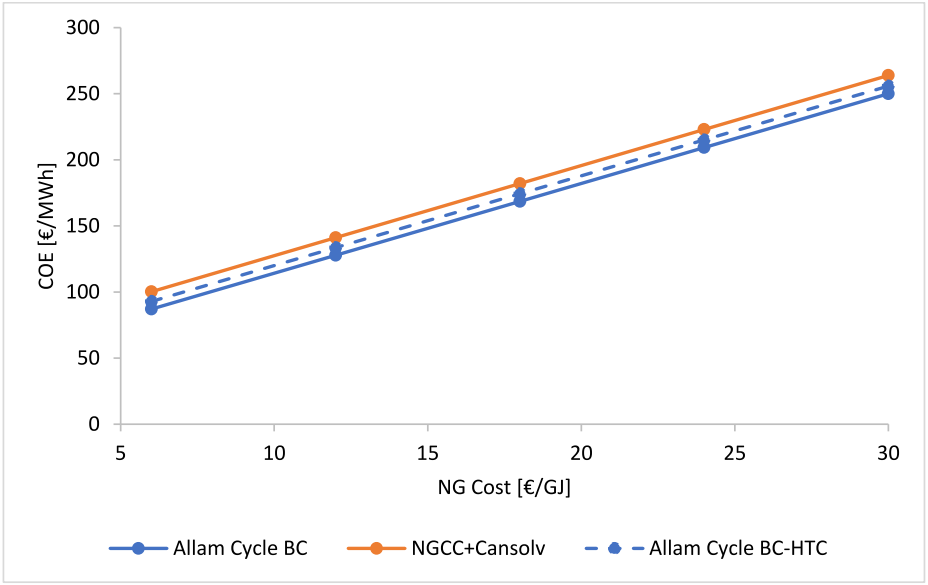

Fig. 16. Sensitivity analysis on the NG cost.

Declaration of competing interest

The authors declare that they have no known competing financial interests or personal relationships that could have appeared to influence the work reported in this paper.

Data availability

Data will be made available on request.

Acknowledgement

None

Appendix

Table A1
Main results of the performance assessment for compressors of all the considered plant sizes.

400 MW plant size	**cpr. 1**	**cpr. 2**	**cpr. 3**	**cpr. 4**	**pump 1**	**oxy pump**	**pump 2**
Isent. work., kJ/kg	19.30	13.50	7.92	6.42	4.84	28.61	25.39
Inlet volum. flow rate, m3/s	18.86	11.89	7.69	4.99	1.81	0.82	1.00
Size paramter, m	0.37	0.32	0.29	0.25	0.16	0.07	0.08
pressure ratio	1.45	1.34	1.23	1.23	1.51	2.60	2.60
rotational speed (RPM)	3000	3000	3000	3000	3000	11000	11000
specific rotational speed	0.83	0.86	1.04	0.98	0.73	0.47	0.57
gearbox	NO	NO	NO	NO	NO	YES	YES
isentropic efficiency	89.74 %	89.31 %	89.04 %	88.53 %	87.18 %	84.18 %	84.77 %
electric efficiency of driver	98.80 %	98.73 %	98.64 %	98.60 %	98.55 %	98.76 %	98.75 %
mechanical efficiency	99.90 %	99.90 %	99.90 %	99.90 %	99.90 %	99.00 %	99.00 %
Electrical power, kW	24151	16992	10014	8188	8264	17731	17654
300 MW plant size	**cpr. 1**	**cpr. 2**	**cpr. 3**	**cpr. 4**	**pump 1**	**oxy pump**	**pump 2**
Isent. work., kJ/kg	14.48	10.13	5.94	4.82	3.63	21.46	19.04
Inlet vol. flow rate, m3/s	14.15	8.92	5.77	3.74	1.36	0.62	0.75
Size paramter, m	0.25	0.22	0.19	0.16	0.12	0.05	0.06
pressure ratio	1.45	1.34	1.23	1.10	1.51	2.60	2.60
rotational speed (RPM)	3000	3000	3000	3000	3000	30000	30000
specific rotational speed	0.51	0.52	0.60	0.58	0.48	0.78	1.08
gearbox	NO	NO	NO	NO	NO	YES	YES
isentropic efficiency	88.56 %	88.08 %	87.72 %	87.25 %	86.20 %	82.81 %	83.56 %
electric efficiency of driver	98.75 %	98.68 %	98.58 %	98.55 %	98.50 %	98.71 %	98.70 %
mechanical efficiency	99.90 %	99.90 %	99.90 %	99.90 %	99.90 %	99.00 %	99.00 %
Electrical Power, kW	18756	13197	7778	6361	6397	14127	13359
200 MW plant size	**cpr. 1**	**cpr. 2**	**cpr. 3**	**cpr. 4**	**pump 1**	**oxy pump**	**pump 2**
Isent. Work, kJ/kg	9.65	6.75	3.96	3.21	2.42	14.31	12.70
Inlet volum. Flow rate, m3/s	9.43	5.95	3.85	2.50	0.91	0.41	0.50
Size paramter, m	0.17	0.15	0.14	0.13	0.06	0.03	0.03
pressure ratio	1.45	1.34	1.23	1.23	1.51	2.60	2.60
rotational speed (RPM)	3000	3000	3000	3000	3000	30000	30000
specific rotational speed	0.25	0.27	0.33	0.34	0.19	0.38	0.35
gearbox	NO	NO	NO	NO	NO	YES	YES
isentropic efficiency	87.29 %	86.91 %	86.77 %	86.50 %	84.22 %	81.44 %	81.36 %
electric efficiency of driver	98.67 %	98.61 %	98.51 %	98.47 %	98.42 %	98.63 %	98.63 %
mechanical efficiency	99.90 %	99.90 %	99.90 %	99.90 %	99.90 %	99.00 %	99.00 %
Electrical power, kW	11985	8749	5522	12761	2951	10266	7989
100 MW plant size	**cpr. 1**	**cpr. 2**	**cpr. 3**	**cpr. 4**	**pump 1**	**oxy pump**	**pump 2**
Isent. Work kJ/kg	4.83	3.38	1.98	1.61	1.21	7.15	6.35
Inlet vol. flow rate, m3/s	4.72	2.97	1.92	1.25	0.45	0.21	0.25
Size paramter, m	0.07	0.06	0.06	0.05	0.03	0.02	0.02
pressure ratio	1.45	1.34	1.23	1.23	1.51	2.60	2.60
rotational speed (RPM)	6000	6000	6000	6000	6000	35000	35000
specific rotational speed	0.15	0.16	0.20	0.20	0.11	0.13	0.13
gearbox	YES	YES	YES	YES	YES	YES	YES
isentropic efficiency	84.59 %	84.21 %	84.06 %	83.78 %	81.55 %	80.07 %	80.05 %
electric efficiency of driver	98.55 %	98.48 %	98.38 %	98.34 %	98.30 %	98.50 %	98.50 %
mechanical efficiency	99.00 %	99.00 %	99.00 %	99.00 %	99.00 %	99.00 %	99.00 %
Electrical power, kW	6579	4629	2727	2226	1705	5198	2092
50 MW plant size	**cpr. 1**	**cpr. 2**	**cpr. 3**	**cpr. 4**	**pump 1**	**oxy pump**	**pump 2**
isent work, kJ/kg	2.41	1.69	0.99	0.80	0.61	3.58	3.17
Inlet vol. flow rate, m3/s	2.36	1.49	0.96	0.62	0.23	0.10	0.13
Size paramter, m	0.13	0.12	0.11	0.09	0.06	0.03	0.03
pressure ratio	1.45	1.34	1.23	1.23	1.51	2.60	2.60
rotational speed (RPM)	8000	8000	8000	8000	8000	40000	40000
specific rotational speed	0.83	0.86	1.03	0.97	0.72	0.66	0.76
gearbox	YES	YES	YES	YES	YES	YES	YES
isentropic efficiency	86.62 %	86.18 %	85.92 %	85.40 %	85.30 %	80.86 %	81.05 %
electric efficiency of driver	98.42 %	98.35 %	98.26 %	98.22 %	98.17 %	98.38 %	98.22 %
mechanical efficiency	99.00 %	99.00 %	99.00 %	99.00 %	99.00 %	99.00 %	99.00 %
Electrical power, kW	3923	1333	1715	1368	1055	2922	3407

Table A2
Thermodynamic properties and composition of the flows for the 99.5 % purity 400 MW Allam cycle. Flow numbers referred to Fig. 1.

Flow #	T [°C]	p [bar]	m [kg/s]	Mol %	CH4	C2H6	C3H8	C4H10-1	C5H12-1	CO2	H2O	O2	N2	Ar
1	15.00	30.00	15.71		0.890	0.070	0.010	0.001	0.000	0.020	0.000	0.000	0.009	0.000
2	40.00	100.80	15.71		0.890	0.070	0.010	0.001	0.000	0.020	0.000	0.000	0.009	0.000
3	151.51	315.60	15.71		0.890	0.070	0.010	0.001	0.000	0.020	0.000	0.000	0.009	0.000
4	705.90	309.99	578.83		0.000	0.000	0.000	0.000	0.000	0.850	0.001	0.133	0.011	0.005
5	705.90	309.99	555.00		0.000	0.000	0.000	0.000	0.000	0.980	0.001	0.001	0.012	0.006
6	1156.90	306.95	1149.54		0.000	0.000	0.000	0.000	0.000	0.916	0.066	0.001	0.011	0.005
7	111.73	309.99	84.66		0.000	0.000	0.000	0.000	0.000	0.980	0.001	0.001	0.012	0.006
8	725.90	30.60	1234.20		0.000	0.000	0.000	0.000	0.000	0.921	0.062	0.001	0.011	0.005
9	63.03	29.83	1234.20		0.000	0.000	0.000	0.000	0.000	0.921	0.062	0.001	0.011	0.005
10	26.00	29.07	1202.23		0.000	0.000	0.000	0.000	0.000	0.980	0.001	0.001	0.012	0.006
11	26.00	29.07	1160.04		0.000	0.000	0.000	0.000	0.000	0.980	0.001	0.001	0.012	0.006
12	26.00	80.00	1160.04		0.000	0.000	0.000	0.000	0.000	0.980	0.001	0.001	0.012	0.006
13	26.00	120.00	639.66		0.000	0.000	0.000	0.000	0.000	0.980	0.001	0.001	0.012	0.006
14	51.05	311.60	555.00		0.000	0.000	0.000	0.000	0.000	0.980	0.001	0.001	0.012	0.006
15	51.05	311.60	84.66		0.000	0.000	0.000	0.000	0.000	0.980	0.001	0.001	0.012	0.006
16	26.00	120.00	520.39		0.000	0.000	0.000	0.000	0.000	0.980	0.001	0.001	0.012	0.006
17	15.00	120.00	58.44		0.000	0.000	0.000	0.000	0.000	0.000	0.000	0.995	0.002	0.003
18	17.40	120.00	578.83		0.000	0.000	0.000	0.000	0.000	0.850	0.001	0.133	0.011	0.005
19	47.95	311.60	578.83		0.000	0.000	0.000	0.000	0.000	0.850	0.001	0.133	0.011	0.005
22	26.00	29.07	42.18		0.000	0.000	0.000	0.000	0.000	0.980	0.001	0.001	0.012	0.006
23	26.00	29.07	31.97		0.000	0.000	0.000	0.000	0.000	0.000	1.000	0.000	0.000	0.000

References

[1] International Energy Agency (IEA), "Energy Technology Perspectives 2020 - Special Report on Carbon Capture Utilisation and Storage," Paris, 2020. doi: 10.1787/208b66f4-en.

[2] International Energy Agency Greenhouse Gas R&D Programme (IEAGHG), "Oxy-Combustion Turbine Power Plants," Cheltenham, UK, 2015. [Online]. Available: https://ieaghg.org/docs/General_Docs/Reports/2015-05.pdf.

[3] James R, Zoelle A, Keairns D, Turner M, Woods M, Kuehn N. Cost and performance baseline for fossil energy plants volume 1: bituminous coal and natural gas to electricity. NETL technical report, NETL-PUB-22638 2019. https://doi.org/10.2172/1893822.

[4] Yang HJ, Kang DW, Ahn JH, Kim TS. Evaluation of design performance of the semi-closed oxy-fuel combustion combined cycle. J Eng Gas Turbines Power 2012;134 (11):Nov. https://doi.org/10.1115/1.4007322.

[5] Allam RJ, et al. High efficiency and low cost of electricity generation from fossil fuels while eliminating atmospheric emissions, including carbon dioxide. Energy Procedia 2013;37:1135–49. https://doi.org/10.1016/j.egypro.2013.05.211.

[6] Allam RJ, Fetvedt JE, Forrest BA, Freed DA. The OXY-fuel, supercritical CO2 allam cycle: New cycle developments to produce even lower-cost electricity from fossil fuels without atmospheric emissions. Proc ASME Turbo Expo 2014. https://doi.org/10.1115/GT2014-26952.

[7] Allam R, et al. Demonstration of the allam cycle: an update on the development status of a high efficiency supercritical carbon dioxide power process employing full carbon capture. Energy Procedia 2017;114:5948–66. https://doi.org/10.1016/j.egypro.2017.03.1731.

[8] R. J. Allam, M. R. Palmer, and G. W. Brown, 2010 "System and method for high efficiency power generation using a carbon dioxide circulating working fluid.," U. S. Patent No. 20110179799A1.

[9] Allam RJ, Fetvedt JE, Forrest BA, Freed DA. The oxy-fuel, supercritical CO2 allam cycle: new cycle developments to produce even lower-cost electricity from fossil fuels without atmospheric emissions. Proc ASME Turbo Expo 2014;3B. https://doi.org/10.1115/GT2014-26952.

[10] "NET Power Website." https://netpower.com/news/ (accessed Jun. 28, 2022).

[11] R. J. Allam, B. A. Forrest, and J. E. Fetvedt, 2017 "Method and system for power production with improved efficiency," US patent US10711695B2.

[12] Scaccabarozzi R, Gatti M, Martelli E. Thermodynamic analysis and numerical optimization of the NET Power oxy-combustion cycle. Appl Energy 2016;178: 505–26. https://doi.org/10.1016/j.apenergy.2016.06.060.

[13] Wimmer K, Sanz W. Optimization and comparison of the two promising oxy-combustion cycles NET Power cycle and Graz Cycle. Int J Greenh Gas Control 2020;99:103055. https://doi.org/10.1016/j.ijggc.2020.103055.

[14] Rogalev A, Grigoriev E, Kindra V, Rogalev N. Thermodynamic optimization and equipment development for a high efficient fossil fuel power plant with zero emissions. J Clean Prod 2019;236:117592. https://doi.org/10.1016/j.jclepro.2019.07.067.

[15] Colleoni L, Sindoni A, Ravelli S. Comprehensive thermodynamic evaluation of the natural gas-fired allam cycle at full load. Energies 2023;16(6):2597. https://doi.org/10.3390/en16062597.

[16] Mitchell C, Avagyan V, Chalmers H, Lucquiaud M. An initial assessment of the value of Allam Cycle power plants with liquid oxygen storage in future GB electricity system. Int J Greenh Gas Control Aug. 2019;87:1–18. https://doi.org/10.1016/J.IJGGC.2019.04.020.

[17] L. Toby, "Developments in oxyfuel combustion of coal," *IEA Clean Coal Centre, CCC/240, London, United Kingdom*, no. 10, pp. 1–122, 2014.

[18] Zhu Z, Chen Y, Wu J, Zhang S, Zheng S. A modified Allam cycle without compressors realizing efficient power generation with peak load shifting and CO2 capture. Energy 2019;174:478–87. https://doi.org/10.1016/J.ENERGY.2019.01.165.

[19] Yu H, Gundersen T, Gençer E. Optimal liquified natural gas (LNG) cold energy utilization in an Allam cycle power plant with carbon capture and storage. Energy Convers Manag 2021;228:113725. https://doi.org/10.1016/J.ENCONMAN.2020.113725.

[20] Wang K, sen Wang S. Thermodynamic analysis of a comprehensive energy utilization system for natural gas pressure reduction stations based on Allam cycle. Appl. Therm. Eng. 2022;205:118033. https://doi.org/10.1016/J.APPLTHERMALENG.2021.118033.

[21] Zhang X, Yu L, Li M, Song P. Simulation of a supercritical CO2 recompression cycle with zero emissions. J Energy Eng 2020;146(6):04020059. https://doi.org/10.1061/(ASCE)EY.1943-7897.0000711.

[22] Chan W, Lei X, Chang F, Li H. Thermodynamic analysis and optimization of Allam cycle with a reheating configuration. Energy Convers Manag 2020;224:113382. https://doi.org/10.1016/J.ENCONMAN.2020.113382.

[23] Wang S, Fernandes D, Xu Q, Chen D. New conceptual design of an integrated allam-cycle power complex coupling air separation unit and ammonia plant. Ind Eng Chem Res 2021;60(49):18007–17.

[24] Luo J, Emelogu O, Morosuk T, Tsatsaronis G. Exergy-based investigation of a coal-fired allam cycle. Energy 2021;218:119471. https://doi.org/10.1016/J.ENERGY.2020.119471.

[25] Xin T, Xu C, Liu Y, Yang Y. Thermodynamic analysis of a novel zero carbon emission coal-based polygeneration system incorporating methanol synthesis and Allam power cycle. Energy Convers Manag 2021;244:114441. https://doi.org/10.1016/J.ENCONMAN.2021.114441.

[26] Xin T, Xu C, Liu X, Li S, Yang Y. Thermodynamics study of a solar hybrid allam cycle integrated with methane reforming. AIP Conf Proc 2020. https://doi.org/10.1063/5.0035144.

[27] Scaccabarozzi R, Gatti M, Campanari S, Martelli E. Solid oxide semi-closed CO2 cycle: a hybrid power cycle with 75% net efficiency and zero emissions. Appl Energy 2021;290:116711. https://doi.org/10.1016/J.APENERGY.2021.116711.

[28] Sasaki T, Itoh M, Maeda H, Tominaga J, Saito D, Niizeki Y. Development of turbine and combustor for a semi-closed recuperated brayton cycle of supercritical carbon dioxide. Am Soc Mech Eng Power Div POWER 2017;1. https://doi.org/10.1115/POWER-ICOPE2017-3419.

[29] Scaccabarozzi R, Martelli E, Gatti M, Chiesa P, Pini M, De Servi CM. Conceptual thermo-fluid dynamic design of the cooled supercritical co 2 turbine for the allam cycle. Int. Conf. Appl. Energy 2019:1–8. https://doi.org/10.46855/energy-proceedings-4334.

[30] Scaccabarozzi R, Gatti M, Martelli E. Thermodynamic optimization and part-load analysis of the NET power cycle. Energy Procedia 2017;114:551–60. https://doi.org/10.1016/J.EGYPRO.2017.03.1197.

[31] Zaryab SA, Scaccabarozzi R, Martelli E. Advanced part-load control strategies for the Allam cycle. Appl Therm Eng 2020;168(July):114822. https://doi.org/10.1016/j.applthermaleng.2019.114822.

[32] EUROPEAN INDUSTRIAL GASES ASSOCIATION, "OXYGEN PIPELINE AND PIPING SYSTEMS," 2020. [Online]. Available: chrome-extension://efaidnbmnnnibpcajpcglclefindmkaj/https://www.eiga.eu/uploads/documents/DOC013.pdf.

[33] Mantovani M, Chiesa P, Valenti G, Gatti M, Consonni S. Supercritical pressure–density–temperature measurements on CO2–N2, CO2–O2 and CO2–Ar binary mixtures. J Supercrit Fluids 2012;61:34–43. https://doi.org/10.1016/j.supflu.2011.09.001.
[34] Patel MR, Holste JC, Hall KR, Eubank PT. Thermophysical properties of gaseous carbon dioxide water mixtures. Fluid Phase Equilib 1987;36:279–99. https://doi.org/10.1016/0378-3812(87)85029-X.
[35] Yang X, Wang Z, Li Z. Accurate density measurements on ternary mixtures (Carbon Dioxide + Nitrogen + Argon) at temperatures from (323.15 to 423.15) K with pressures from (3 to 31) MPa using a single-sinker densimeter. J Chem Eng Data 2015;60(11):3353–7. https://doi.org/10.1021/acs.jced.5b00625.
[36] Sala L, Zaryab SA, Chiesa P, Martelli E. Comparison and optimization of CO2 purification units for CCS applications. Int J Greenh Gas Control 2024;136:104193. https://doi.org/10.1016/j.ijggc.2024.104193.
[37] Lasala S, Chiesa P, Privat R, Jaubert JN. VLE properties of CO2 – Based binary systems containing N2, O2 and Ar: experimental measurements and modelling results with advanced cubic equations of state. Fluid Phase Equilib 2016;428:18–31. https://doi.org/10.1016/j.fluid.2016.05.015.
[38] "Aspen Technology, Inc." https://www.aspentech.com/en (accessed Feb. 21, 2024).
[39] Balje OE, Japikse D. Turbomachines—a guide to design selection and theory. J Fluids Eng 1981;103(4):644. https://doi.org/10.1115/1.3241788.
[40] Romei A, Gaetani P, Giostri A, Persico G. The role of turbomachinery performance in the optimization of supercritical carbon dioxide power systems. J. Turbomach. 2020;142(7). https://doi.org/10.1115/1.4046182.
[41] Gibson SM. Oxygen plants for gasification. New Horizons Gasif 2014:1–9.
[42] Mylavarapu SK, Sun X, Christensen RN, Unocic RR, Glosup RE, Patterson MW. Fabrication and design aspects of high-temperature compact diffusion bonded heat exchangers. Nucl Eng Des 2012;249:49–56. https://doi.org/10.1016/j.nucengdes.2011.08.043.
[43] Martelli E, Girardi M, Chiesa P. Breaking 70% net electric combined cycle efficiency with CMC gas turbine blades. Proc ASME Turbo Expo 2022. https://doi.org/10.1115/GT2022-81118.
[44] Cameretti MC, Langella G, Sabino S, Tuccillo R. Modeling of a hybrid solar micro gas-turbine power plant. Energy Procedia 2015;82:833–40. https://doi.org/10.1016/j.egypro.2015.11.820.
[45] "Baker Huges Website." https://www.bakerhughes.com/ (accessed Jun. 28, 2022).
[46] "Siemens Website." https://www.siemens.com/global/en.html (accessed Jun. 28, 2022).
[47] "ABB Group Website." https://global.abb/group/en (accessed Jun. 28, 2022).
[48] V. White and R. J. Allam, "Purification of carbon dioxide," U.S. Patent No. 20080173585A1, 2008.
[49] Strube R, Manfrida G. CO2 capture in coal-fired power plants-Impact on plant performance. Int J Greenh Gas Control 2011;5(4):710–26. https://doi.org/10.1016/J.IJGGC.2011.01.008.
[50] Sala L, Zaryab SA, Chiesa P, Romano M, Martelli E. Optimization of flash-separation based CO2 purification units. Comput Aided Chem Eng 2023;52:3097–102. https://doi.org/10.1016/B978-0-443-15274-0.50494-7.
[51] "Linde Engineering Website." https://www.linde-engineering.com/en/images/Air-separation-plants-history-and-technological-progress-2019_tcm19-457349.pdf.
[52] "Air Liquide Website." https://www.airliquide.com/group/press-releases-news/2018-02-01/south-africa-air-liquide-starts-worlds-largest-oxygen-production-unit.
[53] Higginbotham P, White V, Fogash K, Guvelioglu G. Oxygen supply for oxyfuel CO2 capture. Int J Greenh Gas Control 2011;5:S194–203. https://doi.org/10.1016/j.ijggc.2011.03.007.
[54] IEA Greenhouse Gas R&D Programme (IEA GHG), "Improved oxygen production technologies," Cheltenham, UK, 2007.
[55] Horlock JH, Watson DT, Jones TV. Limitations on gas turbine performance imposed by large turbine cooling flows. J Eng Gas Turbines Power 2001;123(3):487–94. https://doi.org/10.1115/1.1373398.
[56] El-Masri MA. On thermodynamics of gas-turbine cycles: part 2—a model for expansion in cooled turbines. J Eng Gas Turbines Power 1986;108(1):151–9. https://doi.org/10.1115/1.3239862.
[57] Jordal K, Torbidoni L, Massardo AF. Convective blade cooling modelling for the analysis of innovative gas turbine cycles. Proc ASME Turbo Expo 2001. https://doi.org/10.1115/2001-GT-0390.
[58] Scaccabarozzi R, Martelli E, Pini M, De Servi CM, Chiesa P, Gatti M. "A code for the preliminary design of cooled supercritical CO2 turbines and application to the allam cycle,". J. Eng. Gas Turbines Power 2022;144(3). https://doi.org/10.1115/1.4052146/1115812.
[59] Chiesa P, Macchi E. A thermodynamic analysis of different options to break 60% electric efficiency in combined cycle power plants. J Eng Gas Turbines Power 2004;126(4):770–85. https://doi.org/10.1115/1.1771684.
[60] Dipierro V, Martinelli M, Persico G, Martelli E. Mean-line design and optimization of axial-flow turbines based on mixed integer nonlinear programming. Proc ASME Turbo Expo 2022. https://doi.org/10.1115/GT2022-82688.
[61] R. A. Bidkar *et al.*, "Conceptual Designs of 50MWe and 450MWe Supercritical CO2 Turbomachinery Trains for Power Generation from Coal. Part 1: Cycle and Turbine," 2016, Accessed: Jun. 23, 2022. [Online]. Available: https://www.semanticscholar.org/paper/Conceptual-Designs-of-50MWe-and-450MWe-CO2-Trains-Bidkar-Mann/b97f75aebead535920f580b5b5a432b08f7c9ab0.
[62] "Renk MAAG gearboxes catalogue." https://renk-maag.ch/wp-content/uploads/post_151/RENK_MAAG_Turbo_Gearboxes.pdf (accessed Nov. 14, 2021).
[63] Ligrani P, Potts G, Fatemi A. Endwall aerodynamic losses from turbine components within gas turbine engines. Propuls Power Res 2017;6(1):1–14. https://doi.org/10.1016/j.jppr.2017.01.006.
[64] Haseli Y, Sifat NS. Performance modeling of Allam cycle integrated with a cryogenic air separation process. Comput Chem Eng 2021;148:107263. https://doi.org/10.1016/j.compchemeng.2021.107263.
[65] Linnhoff B, Flower JR. Synthesis of heat exchanger networks: I. systematic generation of energy optimal networks. AIChE J 1978;24(4):633–42. https://doi.org/10.1002/aic.690240411.
[66] Shiferaw D, Carrero JM, Le Pierres R. "Economic analysis of SCO2 cycles with PCHE recuperator design optimisation". 5th Int Symp - Supercrit CO2 Power Cycles 2016:1–13.
[67] Embaye M. Heat Exchangers for Supercritical CO2 Power Application. Presentation made for the ASME TurboExpo 2021 conference tutorial. 2021.
[68] Bergman TL, Lavine AS, Incropera FP, Dewitt DP. Fundamentals of Heat and Mass Transfer. 7th ed. John Wiley & Sons; 2011.
[69] Alfarawi S, Abdel-Moneim SA, Bodalal A. Experimental investigations of heat transfer enhancement from rectangular duct roughened by hybrid ribs. Int J Therm Sci 2017;118(April):123–38. https://doi.org/10.1016/j.ijthermalsci.2017.04.017.
[70] Bynum ML, et al. Pyomo — Optimization Modeling in Python. 3rd ed. Springer International Publishing; 2021.
[71] Tawarmalani M, Sahinidis NV. A polyhedral branch-and-cut approach to global optimization. Math Program 2005;103(2):225–49. https://doi.org/10.1007/s10107-005-0581-8.
[72] Martelli E, Kreutz T, Consonni S. Comparison of coal IGCC with and without CO2 capture and storage: shell gasification with standard vs. partial water quench. Energy Procedia 2009;1(1):607–14. https://doi.org/10.1016/j.egypro.2009.01.080.
[73] Elsido C, Martelli E, Kreutz T. Heat integration and heat recovery steam cycle optimization for a low-carbon lignite/biomass-to-jet fuel demonstration project. Appl Energy 2019;239:1322–42. https://doi.org/10.1016/j.apenergy.2019.01.221.
[74] Market Observatory for Energy, "Quarterly report on European gas markets," 2021. [Online]. Available: https://energy.ec.europa.eu/data-and-analysis/market-analysis_en.
[75] "ICE Website." https://www.theice.com/index (accessed Dec. 21, 2022).
[76] Smith E, Morris J, Kheshgi H, Teletzke G, Herzog H, Paltsev S. The cost of CO2 transport and storage in global integrated assessment modeling. Int J Greenh Gas Control 2021;109:103367. https://doi.org/10.1016/j.ijggc.2021.103367.
[77] "The Chemical Engineering Plant Cost Index, Chemical Engineering." https://www.chemengonline.com/pci-home (accessed Dec. 11, 2023).
[78] Lasala S, Chiesa P, Privat R, Jaubert JN. Measurement and prediction of multi-property data of CO2-N2-O2-CH4 mixtures with the 'Peng-Robinson + residual Helmholtz energy-based' model. Fluid Phase Equilib 2017;437:166–80. https://doi.org/10.1016/j.fluid.2017.01.016.